



1 Merging modelled and reported flood impacts in Europe in a 2 combined flood event catalogue, 1950-2020

3 Dominik Paprotny¹, Belinda Rhein^{1,2}, Michalis I. Voudoukas³, Paweł Terefenko⁴, Francesco Dottori⁵,
4 Simon Treu¹, Jakub Śledziowski⁴, Luc Feyen⁶, and Heidi Kreibich⁷

5 ¹ Potsdam Institute for Climate Impact Research (PIK), Member of the Leibniz Association, P.O. Box 60 12 03, 14412
6 Potsdam, Germany, ² Humboldt-Universität zu Berlin, Berlin, Germany, ³ University of the Aegean, Department of Marine
7 Sciences, Mytilene, Greece, ⁴ Institute of Marine and Environmental Sciences, University of Szczecin, Adama Mickiewicza
8 16, 70-383 Szczecin, Poland, ⁵ CIMA Research Foundation, Savona, Italy, ⁶ European Commission, Joint Research Centre
9 (JRC), Ispra, Italy, ⁷ GFZ German Research Centre for Geosciences, Section Hydrology, Potsdam, Germany
10 *Correspondence to:* Dominik Paprotny (dominik.paprotny@pik-potsdam.de)
11

12 **Abstract.** Long-term trends in flood losses are regulated by multiple factors including climate variation, demographic
13 dynamics, economic growth, land-use transitions, reservoir construction and flood risk reduction measures. Attribution of
14 those drivers through the use of counterfactual scenarios of hazard, exposure or vulnerability first requires a good
15 representation of historical events, including their location, intensity and the factual circumstances in which they occurred.
16 Here, we develop a chain of models that is capable of recreating riverine, coastal and compound floods in Europe between
17 1950 and 2020 that had a potential to cause significant socioeconomic impacts. This factual catalogue of almost 15,000 such
18 events was scrutinised with historical records of flood impacts. We found that at least 10% of them had led to significant
19 socioeconomic impacts (including fatalities) according to available sources. The model chain was able to capture events
20 responsible for 96% of known impacts contained in the HANZE flood impact database in terms of persons affected and
21 economic losses, and for 81% of fatalities. The dataset enables studying drivers of vulnerability and flood adaptation due to a
22 large sample of events with historical impact data. The model chain can further be used to generate counterfactual events,
23 especially related to climate change and human influence on catchments.

24 1 Introduction

25 Flood risk is constantly evolving and influenced by a wide array of drivers, related to atmospheric, land surface and socio-
26 economic processes (Merz et al., 2021). Recent decades have been identified as a particularly flood-rich period along European
27 rivers (Blöschl et al., 2020) and increasing sea levels are expected to exacerbate coastal flood risk (Voudoukas et al., 2017,
28 2023, Nicholls et al., 2021). At the same time exposure is growing rapidly (Paprotny et al., 2018b, Rentschler et al., 2023) and
29 mitigation actions are implemented in reaction to floods (Kreibich et al., 2022). Disentangling the different risk drivers requires
30 considerable modelling effort to reconstruct the factual circumstances surrounding the occurrence of floods and modelling



31 them again under alternative (counterfactual) conditions (Scussolini et al., 2023). Such analyses enable impact attribution, i.e.
32 linking changes in impacts with their likely causes. It can then provide information on long-term development of risk, which
33 in turn has implications on cost-benefit analyses or risk management planning (Kreibich et al., 2019).
34 The recent Sixth Assessment Report of the Intergovernmental Panel on Climate Change, in the chapter on Europe (Bednar-
35 Friedl et al., 2022), indicated low confidence in trends in riverine and coastal flood impacts in the past half-century, even if
36 some increase was detected for parts of the continent. The report contained very limited information on attribution, but this
37 gap is being slowly filled by new studies. For example, Sauer et al. (2021) quantified hazard, exposure and vulnerability
38 changes for flood events globally, finding that for Europe the increase in flood losses was driven almost entirely by exposure,
39 with some small decline in hazard and vulnerability. Though the timeframe of the study was short (1980–2010), it highlighted
40 the role of exposure similarly to Paprotny et al. (2018b), who presented exposure-adjusted losses for 1870–2016 (with
41 consideration for gaps in flood impact reporting), finding no upward trend in economic losses and a strong decline in fatalities.
42 Long-run global data on climatic and socioeconomic drivers under factual and counterfactual scenarios are available from the
43 Inter-Sectoral Model Intercomparison Project, or ISIMIP 3a (Frieler et al., 2024), but they mostly have coarse resolution that
44 is not easily applicable to Europe and have not yet been used for flood impact attribution. Impact attribution of European
45 floods was also carried out with a case study-based, semi-quantitative approach of comparing “paired events”, i.e. floods that
46 have occurred in the same area some years apart (Kreibich et al., 2023). This approach has an advantage mainly in the context
47 of drawing practical conclusions for flood adaptation (Kreibich et al., 2019). Studies that derived projections of future flood
48 risk in Europe have indicated that all three components of risk play an important role in determining changes in the impact
49 magnitude (Rojas et al., 2013, Vousdoukas et al., 2018, Steinhausen et al., 2022, Schoppa et al., 2024).
50 Particular effort is needed in reconstructing the intensity and spatial footprint of flood events. For instance, the loss-
51 normalisation study of Paprotny et al. (2018b) used 100-year riverine and coastal flood hazard maps as proxies for impact
52 zones within subnational regions indicated as affected in the HANZE database (Paprotny et al., 2018a). This approach did not
53 include the effect of climate change, human influence on catchments or simply the variation in return period of different events.
54 There have been attempts to reconstruct past river floods for North America (Wing et al., 2021) or storm surge footprints
55 globally (Enríquez et al., 2020), but none specifically for Europe. Satellite-derived flood footprints can also be linked to impact
56 records, as in Mester et al. (2023), but such datasets cover only a short timeframe and do not resolve the problem of generating
57 a counterfactual hazard scenario.

58 In this study we develop a modelling chain to generate a factual flood catalogue for 42 European countries covering the period
59 1950–2020, which could be further used to run counterfactual scenarios. We only cover the factual scenarios and focus on
60 deriving the best possible reconstruction of past riverine, coastal and compound floods. The main metric of success of the
61 modelling chain is its ability to correctly derive the time, location and intensity of 2037 actual floods contained in the HANZE
62 flood impact database (Paprotny et al., 2023). We further aim at deriving not only the floods that caused significant
63 socioeconomic impacts, but also those that did not happen despite their hydrological extremity due to existing flood protection,
64 as this could later be used to quantify the level of European flood protection.



65 Thanks to the availability of new high-resolution estimates of past population and economic exposure (Paprotny and Mengel,
66 2023), we narrow down our catalogue of floods only to those with significant socioeconomic impact potential, rather than
67 those which were extreme only from a hydrological perspective. This enables comparison with historical records of flood
68 impacts and classifying the modelled events in accordance to their real-life consequences (or lack thereof). Finally, the focus
69 is on coastal, compound and slow-onset riverine flooding. Flash flood events occurring in small catchments (i.e. with an
70 upstream area below 100 km²) are not considered in our analysis due to the insufficient resolution of the riverine flood models
71 available for Europe. Furthermore, we explicitly omit urban floods resulting from insufficient storm drainage rather than from
72 channel overflow.

73 The paper provides a short method overview in section 2.1, which is followed by details on the coastal (2.2) and riverine (2.3)
74 components of the modelling chain, which are brought together for a final flood catalogue compared with historical records
75 (2.4). Validation of the hydrological hazard follows in the next sections (2.5, 3.1), with an overview of risk indicators derived
76 from the catalogue (3.2) and finally comparison between modelled and observed flood impacts (3.3). The discussion analyses
77 the limitations and uncertainties of both the modelled (4.1) and observational data (4.2), before drawing conclusions and
78 highlighting possible applications of the flood catalogue (section 5).

79 **2 Methods**

80 **2.1 Overview**

81 Simulating riverine and coastal floods requires different modelling approaches. First we derive extreme river discharges and
82 coastal water levels, then we apply a common approach to produce flood intensity maps, compute damages, and aggregate
83 the results spatiotemporally. Compound floods are generated by combining the results of the two strands of modelling work,
84 therefore we run the coastal model first, and compound floods are considered as part of the riverine component, drawing on
85 the previous coastal results. The methodology is briefly summarised in Table 1.

86



87 **Table 1. Summary of the methodology, sections with the corresponding descriptions are given in square brackets.**

Step	Coastal floods	Riverine floods
Input climate data	ERA5, interpolated to 0.11° rotated grid [2.2.1]	ERA5-Land, statistically downscaled and bias adjusted to 1 arc min [2.3.1]
Hydrodynamic simulations	Delft3D storm surge height simulation with external data for total water level (hourly) [2.2.2]	LISFLOOD river discharge (Q) simulation (6-hourly) [2.3.2]
Deriving extreme events	TWL > 99.6 th percentile per coastal segment [2.2.3]	Q > 98 th percentile per river grid cell [2.3.3]
	Merging in time (+/- 2 days) and space (NUTS3 regions), including derivation of compound events [2.2.3, 2.3.3]	
Estimating flood footprint	If TWL/Q > 2-year return period, water depth interpolated from a set of flood hazard maps (100 m resolution) [2.2.4, 2.3.4]	
Aggregating flood events	All significantly affected NUTS3 regions aggregated per country using +/- one day window [2.4.1]	
Potential loss modelling	Persons affected, fatalities and economic loss computed from 100 m exposure grid and damage functions [2.4.1]	
Filtering and analysis of flood events	Removing events with low potential impacts	
	Intersecting remaining events with historical impact databases [2.4.2]	
	Comparing modelled event catalogue with other historical records [2.4.3]	
Validation	River discharges, storm surge heights and flood footprints [2.5, 3.1]	
Further analysis	See sections 3.2 and 3.3	

88
 89 In Table 1, the aggregation of extreme discharge or water levels spatially by using NUTS3 regions is mentioned. This refers
 90 to the European Union's (EU) Nomenclature of Territorial Units for Statistics (NUTS). This classification has 4 levels (0, 1,
 91 2, 3), in which 0 is the national level and 3 is the finest sub-regional division. NUTS3 regions are usually administrative
 92 divisions, though at times statistical (analytical) regions are used instead, by amalgamating smaller administrative units
 93 (Eurostat, 2022). Due to its relevance for determining regional policy, data dissemination, and socioeconomic analyses in the
 94 EU, we use this classification as our principal unit of analysis. This further enables direct comparison with the HANZE flood
 95 impact catalogue, which contains data on 2037 reported floods in the study area since 1950, including footprints defined at
 96 NUTS3 level (Paprotny et al., 2023). HANZE also includes exposure and other subnational statistics at the same resolution
 97 (Paprotny and Mengel, 2023). The generation of a high-resolution boundary map of 1422 NUTS3 regions, version 2010, or
 98 their equivalents, is described in Paprotny and Mengel (2023). We further aggregate flood events at national level for
 99 comparison with reported impacts, as this is the typical resolution in which such information is provided. Consequently, the
 100 catalogue is not specific for river catchments or sea basins (as in e.g. Diederer et al., 2019), but for countries and their
 101 subdivisions.

102 It should be highlighted that the catalogue represents possible floods without considering structural flood protection measures,
 103 hence they are not included in the potential flood footprint estimates. Due to the very limited information on present or past
 104 protection standards, adding estimates of those would potentially create large inaccuracies by filtering out events that happened
 105 in history.



106 2.2 Coastal model

107 2.2.1 Climate data

108 We model storm surge heights driven by hourly 10-m wind speeds (u and v component) and surface air pressure, drawing data
109 from the latest ERA5 climate reanalysis (Hersbach et al., 2020). The data were downloaded at a resolution of 0.25°
110 (approximately 28 km at the equator) and then interpolated using first-order conservative remapping (Jones, 1999) to a 0.11°
111 rotated-pole (12.5 km) grid used in our storm surge model, which in turn is the same as the CORDEX grid used in European
112 climate projections (Jacob et al., 2014). Apart from the interpolation, no further adjustments were made to the data.

113 2.2.2 Sea level estimation

114 The principal component of extreme sea levels are storm surges, which we estimate through a continuous simulation in
115 Delft3D. This hydrodynamic model is commonly applied in continental- or global-scale surge modelling (e.g. Vousdoukas et
116 al., 2016a, Ganguli et al., 2020, Muis et al., 2020). The model set-up is the same as described in Paprotny et al. (2016, 2019),
117 with the difference that it is forced by wind and atmospheric pressure fields from ERA5 instead of ERA-Interim. We also
118 carried out a calibration, using the previous calibration as the starting point, by adjusting the sea bottom roughness coefficients
119 for different basins around Europe, and comparing the modelled surge heights with tide gauge observations for years 2011–
120 2019. This recalibration also benefited from much better availability of observational data, which are described in section 2.5,
121 as they are also used to validate the final simulation. Additionally, the timestep of the model was reduced to 15 min, with
122 outputs saved hourly, compared to 30 min and 6 hours, respectively, in the original version. The model was run from 1 January
123 1949, with the first year used only as spin-up. Actual ERA5 data was used in the spin-up phase thanks to recent extension of
124 the dataset to 1940.

125 As storm surge heights are only one component of extreme sea levels, the hourly total water level (L) is the combination of six
126 components:

$$127 \quad L = S + T + W + D + M + G \quad (1)$$

128 Where:

- 129 • S is the hourly storm surge height;
- 130 • T is the hourly tide elevation, computed with pyTMD package (<https://github.com/tsutterley/pyTMD>) from 34 tidal
131 constituents;
- 132 • W is the hourly wave run-up, assumed to be 20% of significant wave height (recommended by U.S. Army Corps of
133 Engineers, 2002, used e.g. in Vousdoukas et al., 2016b);
- 134 • D is the mean dynamic topography defined as the average sea surface height for 1993–2012 above geoid;
- 135 • M is the long-term variation in sea level related to climatic variation (“sea level rise”, SLR), defined as average annual
136 difference from average sea level in year 2000;
- 137 • G is the glacial isostatic adjustment (GIA) computed from long-term historical rate of change.



138 Each component was derived from a different source, as summarised in Table 2.

139

140 **Table 2. Source of data for computing hourly total water level. * coarser global data were used for northernmost coasts of Europe**

Component	Source	Spatial resolution	Reference
Storm surge height	Delft3D simulation (this study)	12.5 km	Paprotny et al. (2016)
Tide elevation	FES2014	1/16°	Lyard et al. (2021)
Wave run-up	ERA5	1/2°	Hersbach et al. (2020)
Mean dynamic topography	Global Ocean Mean Dynamic Topography (combines global CNES-CLS18 and CMEMS2020 for Black and Mediterranean seas)	1/8°	Mulet et al. (2021)
Sea level rise	1950–99: Hourly Coastal water levels with Counterfactual (HCC)	10 km	Treu et al. (2023)
	2000–2020: European Seas Gridded L4 Sea Surface Heights*	1/8°	Taburet et al. (2019)
	2000–2020: Global Ocean Gridded L4 Sea Surface Heights*	1/4°	Pujol et al. (2016)
Glacial isostatic adjustment	ICE-6G_C	1/5°	Argus et al. (2014), Peltier et al. (2015)

141

142 2.2.3 Extracting coastal flood events

143 As the resolution of each dataset that is used to derive the total water level varies, we assign the nearest grid point of each
 144 model to 5884 coastal segments defined in the coastal flood hazard model (Vousdoukas et al., 2016b) with a nearest-neighbour
 145 approach. From the detrended (1950–2020) hourly timeseries, occurrences of water level above the 99.6th percentile were
 146 identified and considered potential coastal floods. Occurrence of water levels below the 99.6th percentile for at least two full
 147 calendar days separated two events from each other. Such thresholds lead to, on average, about five potential flood events per
 148 year. Then, events were aggregated according to NUTS3 regional boundaries, again with the principle that the beginning of
 149 any segment-level flood event in a NUTS3 region has to occur at least two full calendar days after the end of any previous
 150 segment-level event in that region.

151 2.2.4 Deriving coastal flood footprints

152 For each coastal segment in the dataset, an extreme value analysis was carried out using a Generalised Pareto distribution and
 153 a peak-over-threshold approach. This enabled deriving extreme sea level scenarios (return periods of 2, 5, 10, 20, 30, 50, 100,
 154 200, and 500 years) for coastal inundation modelling. This was carried out according to a methodology developed by
 155 Vousdoukas et al. (2016b). Briefly, the maps were generated with the Lisflood-ACC (LFP) model (Bates et al., 2010) applied
 156 at 30 m spatial resolution. In terms of Digital Elevation Model (DEM), we use the recently published GLO-30 DEM (European
 157 Space Agency and Sinergise, 2021) after applying post-processing using global LIDAR observations to further remove vertical
 158 bias, correcting for buildings and vegetation. The description of the GLO-30 post-processing is described in detail in Pronk et
 159 al. (2023). The simulations consider gridded hydraulic roughness values derived from land-use maps (Zanaga et al., 2021).



160 Lisflood-ACC is applied for each coastal segment with the model domain extending up to 200 km landwards in order to ensure
161 the inclusion of all potentially hydrologically connected areas that may lie inland and away from the coast.

162 Total water level of each segment-level flood event is linked with the water level used to generate the flood hazard maps for
163 each segment. In this way, it is possible to interpolate water depths from the stack of hazard maps to event-specific extreme
164 sea levels. This is only done if the water levels for an event exceed a flood threshold, defined as the higher of the two following
165 thresholds:

- 166 • Total water level with a 2-year return period, derived from the Generalised Pareto distribution;
- 167 • Maximum observed total water level minus storm surge height.

168 The first threshold was chosen for consistency with the riverine model as it is akin to the typical definition of a bank-full river
169 discharge. The second threshold was added to avoid overestimating risk in regions (mainly Eastern Mediterranean), where
170 storm surge heights are very low, but wave run-up contributes significantly to extreme sea level.

171 Only grid cells with water depths of at least 10 cm were considered inundated for consistency with riverine flood maps. The
172 individual flood maps for each coastal segment were aggregated within a NUTS3-level event. Finally, only those NUTS3-
173 level events were preserved for further analysis if the potential flood zone was at least 100 ha. As further processing is carried
174 out together with the riverine model, we now describe the river component, and continue explaining the next steps towards the
175 combined flood catalogue in section 2.4.

176 **2.3 Riverine model**

177 **2.3.1 Climate data**

178 We used river discharge from Tilloy et al. (2024) that was modelled using ERA5-Land, which is a downscaled version of
179 ERA5 characterised by 0.1° (approximately 11 km at the equator) resolution (Muñoz-Sabater et al., 2021). It was further
180 statistically downscaled and bias adjusted to 1' (arc minute) resolution using ISIMIP3BASD v3.0.0 method developed by
181 Lange (2019, 2022), using EMO-1 gridded observational data, which is a 1' variant of the EMO-5 dataset developed by
182 Thiemiig et al. (2022). Temperature and precipitation with 6-hourly resolution were used as the primary driver of the
183 hydrological model, while potential evapotranspiration was computed at daily resolution using the LISVAP model by van der
184 Knijff (2006). For details on the preparation of the meteorological data, we refer to Tilloy et al. (2024).

185 **2.3.2 River discharge simulation**

186 River discharges were modelled through continuous simulations using the LISFLOOD hydrological model (Burek et al., 2013)
187 implemented in the European Flood Awareness System, or EFAS (Copernicus Emergency Management Service, 2023). Tilloy
188 et al. (2024) used the latest model set-up, v5.0 (Choulga et al., 2023), and simulated river discharges with meteorological
189 inputs described in section 2.3.1. The EFAS model was run starting 3 January 1950 following the 71-year pre-run. Due to
190 rapid evolution of socioeconomic conditions in the catchments of Europe, the input socioeconomic maps were changed with



191 the start of every new calendar year of the simulation. The evolving socioeconomic conditions included land use (in six
192 classes), reservoirs (based on the year of construction of each dam), and water demand (in four sectors). For details on the
193 river discharge simulation and its validation, we again refer to Tilloy et al. (2024).

194 **2.3.3 Extracting riverine flood events**

195 The output of the river model is a time series of 6-hourly discharge for 7.5 million grid cells. Due to the availability of flood
196 hazard maps for footprint estimation (section 2.3.4), we extract data only for 282,528 grid cells that have an upstream area of
197 at least 100 km². Occurrences of discharge above the 98th percentile (on annual basis) were identified and considered potential
198 riverine floods. Occurrence of water levels below the 98th percentile for at least two full calendar days separated two events
199 from each other. As in the coastal model (section 2.2.3), those thresholds were intended to produce roughly five potential flood
200 events per year in each grid cell. Then, events were aggregated according to NUTS3 regional boundaries, again with the
201 principle that the beginning of any grid cell-level flood event in a NUTS3 region has to occur at least two full calendar days
202 after the end of any previous grid cell-level event in that region.

203 **2.3.4 Deriving riverine and compound flood footprints**

204 For each grid cell in the dataset, an extreme value analysis was carried out using a Generalised Pareto distribution and a peak-
205 over-threshold approach, where the peak discharge was detrended based on annual maximum discharge for 1950–2020. In
206 contrast to the coastal model (section 2.2.4), no additional hydrodynamic modelling was carried out in the riverine model.
207 Instead, the flooding processes were represented using the dataset of flood hazard maps developed by Dottori et al. (2022),
208 which are available for a range of return periods from 10 to 500 years for grid cells with an upstream area above 500 km². The
209 maps were generated with the Lisflood-ACC (LFP) model (Bates et al., 2010), applied at 100 m spatial resolution and driven
210 by hydrological simulations from a previous set-up of EFAS (Arnal et al., 2019). In this study, given the different resolutions
211 of the LISFLOOD simulations and the flood hazard maps, the two datasets were matched according to the procedure described
212 in Dottori et al. (2022).

213 To provide coverage for smaller catchments, the flood maps by Paprotny et al. (2017) were applied for grid cells with an
214 upstream area of 100–499 km². The maps for five scenarios (return periods of 10, 30, 100, 300 and 1000 years) were based on
215 discharges estimated with a Bayesian Network-based model from Paprotny and Morales-Nápoles (2017). The simulations
216 were performed using a one-dimensional ‘steady-state’ hydraulic model Deltares SOBEK to obtain water levels along rivers.
217 Those levels were then used to generate water depth maps over a digital elevation model. The maps use the exact same grid as
218 the ones from Dottori et al. (2022). For details on the methodology and validation of the maps we refer to Paprotny et al.
219 (2017).

220 Peak river discharge per each grid cell during a given potential river flood event was linked with the scenarios used to generate
221 the flood hazard maps so that the appropriate maps were used to interpolate water depths. If the return period of the peak
222 discharge was below 10 years, water depths were extrapolated using two maps with the lowest return periods. No flooding was



223 assumed if the peak discharge was below the empirical 2-year return period derived from detrended 1950–2020 peak discharges
224 of the extracted flood events. This threshold was typically much lower than the 2-year return period derived with the
225 Generalized Pareto distribution.

226 Only grid cells with water depths of at least 10 cm were considered inundated, as in the maps of Dottori et al. (2022). The
227 individual flood maps for each river grid cell were aggregated within a NUTS3-level event. Finally, only those NUTS3-level
228 events were preserved for further analysis if the potential flood zone was at least 100 ha. At this point, the list of NUTS3-level
229 events was compared against the same list from the coastal model. If a river event in a given NUTS3 region occurred at the
230 same time as a coastal event in the same region, a separate “compound” event was created by merging the flood zones of the
231 coastal and riverine events in that region. The compound events are analysed in addition to the individual coastal and riverine
232 events, rather than replacing them. From here, processing of the potential flood events follows a common path for all types of
233 events.

234 **2.4 Combined flood catalogue**

235 **2.4.1 Aggregating and estimating potential losses per event**

236 Almost 250,000 potential flood events at the level of NUTS3 regions are aggregated for each country. One full calendar day
237 separates two country-level events consisting of at least one NUTS3 event. Coastal, riverine, and compound events are each
238 aggregated separately. Each event is characterised by hydrological parameters, such as inundated area, average water depth,
239 duration and return period. The latter is the geometric average of all river grid cells or coastal segments that contribute to the
240 flooded area.

241 Potential losses were estimated by multiplying exposure for each 100 m grid cell within each flood footprint with an appropriate
242 loss function. Exposure per grid cell (population and value of fixed assets) was computed with the HANZE v2.0 exposure
243 model (Paprotny and Mengel, 2023), which estimates historical exposure changes using a combination of rule-based and
244 statistical modelling that enabled downscaling past demographic and economic trends at subnational level into a high-
245 resolution grid. The model provides annual data for years 2000–2020 and 5-yearly timesteps for 1950–2000. Alongside
246 population, the model can generate values of tangible fixed asset stock in euros (constant 2020 prices and exchange rates) in
247 8 sectors (housing, consumer durables, agriculture, forestry, industry, mining, services, infrastructure).

248 Firstly, fatalities were estimated per each 100 m grid cell by multiplying the population with the death probability determined
249 by water depth. Due to the lack of velocity data or dike breach locations, only such a simplified approach can be used here.
250 We opted for the S-shaped depth-fatality function by Boyd et al. (2005) as presented in Jonkman et al. (2008), which shows
251 very low chance of death until water depths of approximately 3 m, i.e.:

$$252 \quad F_d = \frac{0.34}{1 + \exp(20.37 - 6.18d)} \quad (2)$$

253 where F_d is the mortality rate and d is the water depth in m.



254 The second indicator, people affected, is simply the total population within the flood footprint. Finally, economic losses were
255 estimated using a set of depth-damage functions for different economic sectors. We applied the logarithmic-type functions
256 proposed for Europe by Huizinga et al. (2017) that distinguish five sectors: agriculture, industry, commercial, infrastructure,
257 and residential. The functions were applied to the appropriate sector in the exposure model. It should be noted that whenever
258 “economic losses” are mentioned in this paper, they only refer to direct damage to tangible fixed assets, without considering
259 indirect impacts.

260 **2.4.2 Obtaining the final flood catalogue**

261 Estimated flood impacts of each event computed in the previous step were used to further filter the flood event catalogue only
262 to those floods with significant potential for socioeconomic impacts. To qualify for the list, the event had to pass two thresholds
263 simultaneously (Table 3):

- 264 ● Inundated area above a fixed threshold, and
- 265 ● At least one of two socioeconomic impact indicators (computed according to section 2.4.1):
 - 266 ○ people potentially affected above fixed threshold, or
 - 267 ○ potential economic losses above an event-specific threshold.

268 The exact threshold depends on the type of event, and in case of economic losses also on country and year of event, as it was
269 linked to the level of gross domestic product (GDP) per capita (Table 3).

271 **Table 3. Thresholds for selecting flood events with significant potential impacts.**

Threshold	Coastal floods	Riverine and compound floods
Area inundated	1000 ha	2000 ha
People affected	2500	5000
Economic damage	10,000 times GDP per capita (country and year of event)	20,000 times GDP per capita (country and year of event)

272
273 Thresholds in Table 3, as well as those described earlier in the methodology, were selected iteratively based on the following
274 objectives:

- 275 ● Maximise the number of modelled events matching observed events from HANZE;
- 276 ● Maximise the share of one-to-one relationships between modelled and observed events (as opposed to many-to-one
277 or one-to-many relationships);
- 278 ● Minimise the spatial extent of events in terms of affected NUTS3 regions beyond those indicated in HANZE;
- 279 ● Create a list of events large enough for statistical analyses and small enough to allow manual searches of historical
280 records for all events.



281 To help select the thresholds, observed flood events from the following six datasets were matched per country according to
 282 start and end dates:

- 283 • HANZE v2.1 (Paprotny et al., 2023);
- 284 • EM-DAT (Centre for Research on the Epidemiology of Disasters 2023);
- 285 • EEA Flood Phenomena (from 1980 only) (European Environment Agency, 2015);
- 286 • Dartmouth Flood Observatory (from 1985 only) (Brakenridge, 2023);
- 287 • FFEM-DB (from 1980 only) (Papagiannaki et al., 2022);
- 288 • Recorded Flood Outlines (England only) (Environment Agency, 2023).

289 In addition, the HANZE dataset was matched with events below the tested thresholds. Following the above objectives results
 290 in different potential impact thresholds for coastal and riverine floods.

291 2.4.3 Comparing modelled and reported events

292 The modelled flood events of the catalogue were evaluated using gauge records and impact data as well as manual research
 293 involving all kinds of documentary sources. At first, English-language papers and local-language flood catalogues providing
 294 an overview of the hazard in the country were consulted. Then, national disaster databases were searched and the relevant data
 295 was extracted. Papers on case studies of disasters were searched for in both English and the local language of the country being
 296 researched. A keyword-based search in both English and the local language was performed using a web engine to identify
 297 news articles or other online reports mentioning the relevant disasters. In total, 946 major text or data sources were used, 828
 298 of which are listed in the HANZE v2.1 dataset (Paprotny et al., 2023) and the remainder is listed together with the data from
 299 this study. Based on this information on impacts, each event was categorised into one of the classes listed in Table 4.

301 **Table 4. Classification of flood events considering the availability of data sources as well as reported hydrological and socioeconomic**
 302 **impacts.**

Class	Short name	Evaluation result	
		Extreme hydrological event	Inundation with significant socioeconomic impacts
A	Impacts, data	Confirmed by sources	Confirmed by sources (impact data available)
B	Impacts, no data	Confirmed by sources	Confirmed by sources (impact data not available)
C	No impacts	Confirmed by sources	Not confirmed by sources
D	Unknown impacts	Confirmed by sources	No sources available
E	False positive	Not confirmed by sources	Not confirmed by sources or no sources available
F	No information	No sources available	No sources available

303
 304 In applying the classification from Table 4, a decision graph from Fig. 1 was used. In general, in case of complete lack of
 305 gauge data or documentary sources, the event was labelled F (“No information”), meaning that no observational data is
 306 available and therefore modelled data can be neither confirmed or rejected. In case gauge records are available, it was firstly
 307 evaluated if they indicate extreme values. Exceedance of a 2-year return period was considered sufficient to confirm that the
 308 modelled event was an extreme hydrological event in real life. If the threshold was not exceeded at any of the available gauge



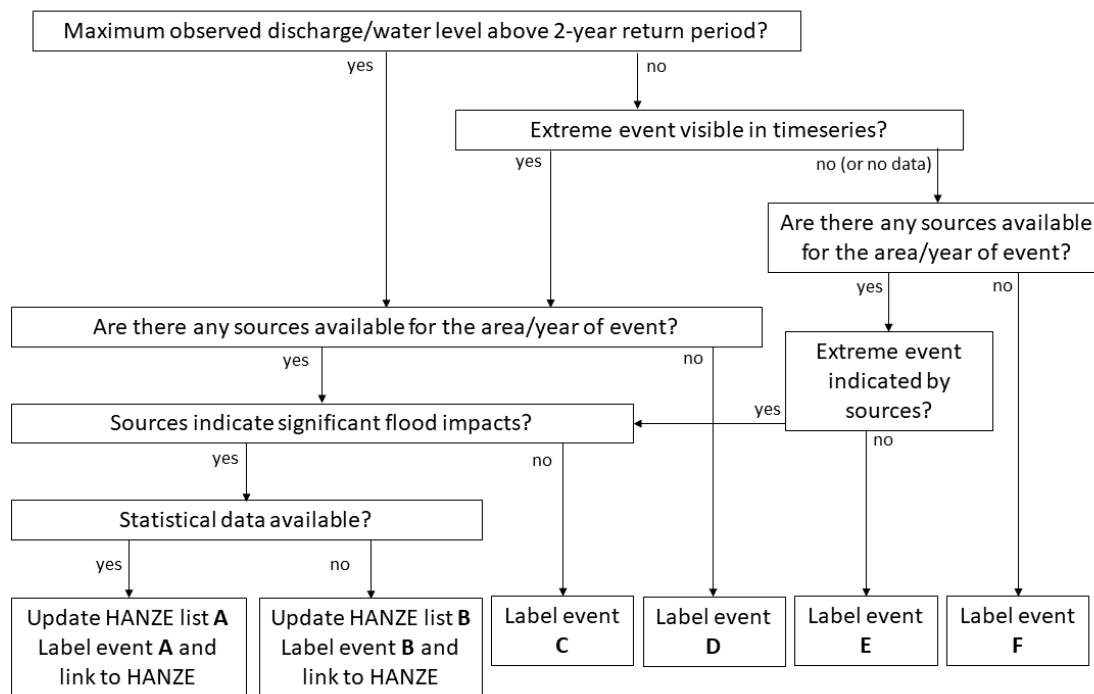
309 stations, the time series was analysed, and the event was considered confirmed as hydrologically extreme if a flood wave was
310 clearly visible at the dates indicated by the model. If no flood wave was visible, the event was considered a “False positive”
311 (label E), i.e. an error of the model that indicates a too high simulated river discharge or sea level. In rare cases, this
312 classification was overridden if documentary sources indicated the occurrence of a flood event.

313 For events confirmed as hydrologically extreme, further analysis concentrated on the occurrence of significant socioeconomic
314 impacts. Here, significant impacts were defined as in the HANZE database (Paprotny et al., 2023), i.e. exceedance of at least
315 one the following thresholds:

- 316 ● At least 1000 ha (10 km²) inundated;
- 317 ● At least one person killed or missing presumed dead;
- 318 ● At least 50 households or 200 people affected by their homes being inundated or who were evacuated;
- 319 ● Losses in monetary terms corresponding to at least 1 million euro in 2020 prices.

320 In case no further information was available, the event was labelled D (“Unknown impacts”). If despite good coverage of
321 sources (e.g. comprehensive local/national flood databases or catalogues), no impacts are mentioned, or in rare cases, direct
322 statement that e.g. a flood emergency did not result in breaching of flood defences, the event was labelled C (“No impacts”).
323 Also, if data on impacts were available, but they did not pass any of the aforementioned thresholds, the event was labelled as
324 “No impacts”. Events with sufficient information on significant impacts were labelled A (“Impact, data”) and incorporated
325 into the HANZE database. However, if statistical data was not accessible, or referred only to a small part of the impacted area,
326 but available descriptions strongly indicated that one of the impact thresholds was likely exceeded, the event was recorded in
327 a separate list of events, labelled B (“Impact, no data”). Available historical information was collected for such an event in a
328 database that is a simplified version of HANZE. Detailed description of the data collected in this database, which is made
329 publicly available with this study, is provided in Appendix A1. It should be noted that a matching of dates and country with
330 historical events was not enough to label the event A or B. For that, at least one NUTS3 region affected during the event had
331 to be correctly identified by the model.

332



333
 334 **Figure 1. Decision graph for classifying flood events.**

335
 336 The final flood catalogue consists of two components: (1) a table with all events, indicating their timing, location, potential
 337 impacts, hydrological parameters and classification, and (2) potential flood footprint maps in vector format. The data contained
 338 in the table are explained in Appendix A2.

339 **2.5 Validation**

340 Validation of river discharges is presented by Tilloy et al. (2024), however we used the 3442 stations containing daily
 341 observations collected for that study for further analysis. The dataset helped us to classify the events in section 2.4.3. Further,
 342 we compared extreme discharges observed during riverine and compound events with modelled discharges. Station data was
 343 obtained in 60% from the Global Runoff Data Centre and in 40% from national public datasets of France, Norway, Poland,
 344 Spain, Sweden and the United Kingdom. The analysis was limited to 2914 stations with an upstream area of at least 100 km²,
 345 located in the affected NUTS3 regions according to the model. If the event duration and available gauge series were both at
 346 least 30 days, the daily discharge was compared using the Kling–Gupta efficiency, or KGE (Gupta et al., 2009), and
 347 Spearman’s coefficient of determination (as Pearson’s is used in the KGE score). Otherwise, an equal amount of days was
 348 added before and after the event, so that at least 30 observations are used. The maximum daily discharges during the event
 349 were also compared.



350 Validation of the hourly storm surge heights, tide elevations and combined water level was done using 428 tide gauges. Almost
351 all stations (413) were gathered from GESLA v3 dataset (Haigh et al., 2023), but for better coverage of the eastern
352 Mediterranean Sea it was complemented with 7 stations from Poseidon System (2023), and for the southern Baltic Sea with 8
353 stations from the Institute of Meteorology and Water Management – National Research Institute (2023). Apart from validation
354 for all available time series, an event-based validation was done as for river discharges. The default time window for the
355 comparison between modelled and observed data was 7 days, unless the event had a longer duration.
356 Finally, the modelled flood footprints were compared with satellite-derived footprints from the Global Flood Database (GFD,
357 Tellman et al., 2021). The footprints were converted into vector layers, with permanent water bodies removed from them, as
358 per data contained in GFD. Only footprints within NUTS3 regions indicated as affected in the HANZE database were included
359 in the analysis. Population affected within the footprints was derived from HANZE population maps. Flooded area and
360 population affected based on footprints from this study and GFD were compared with reported impacts. Additionally, all flood
361 events in the catalogue with comparative reported impact data were analysed for the difference in modelled and reported
362 impacts. Ideally, all modelled impacts should be higher than what was reported, as the intention of the catalogue is to generate
363 potential footprints that do not consider flood protection. Finally, footprints from this study and GFD were intersected to derive
364 the hit rate, i.e. share of the satellite footprints correctly reproduced by the model. This is a similar approach that was used to
365 validate flood hazard maps that are the basis of the modelled footprints (Vousdoukas et al., 2016b, Paprotny et al., 2017,
366 Dottori et al., 2022).

367 **3 Results**

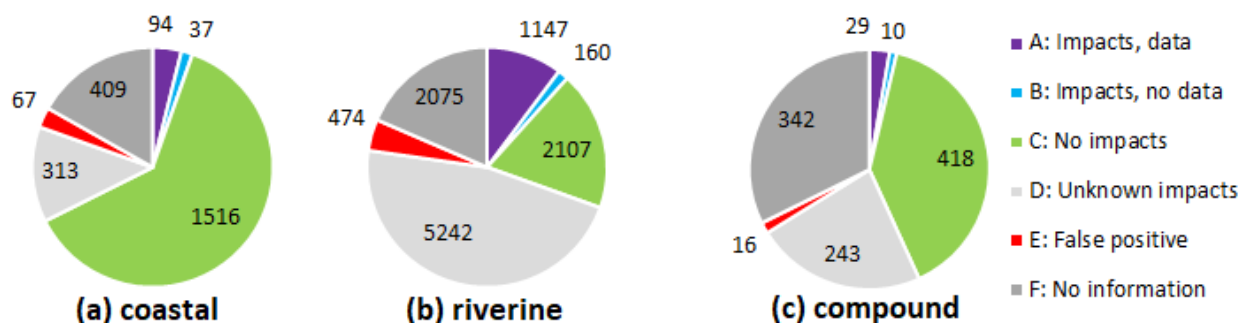
368 **3.1 Flood event catalogue**

369 **3.1.1 Modelled impacts by classification**

370 The final catalogue includes 2436 coastal, 11,205 riverine, and 1058 compound events with significant potential for
371 socioeconomic impacts (Fig. 2). This already indicates a significant proportion of coastal and riverine events might be
372 compound events. The spatial location and timeframe of events was matched with at least some gauge observations for 63%
373 of coastal and 72% of riverine events. By applying the 2-year return period threshold to observational data, it was possible to
374 immediately confirm that 40% of coastal and 45% of riverine events were hydrologically extreme. Further confirmations were
375 obtained through analysis of gauge timeseries and documentary records, increasing the confirmation rate to 80% for coastal,
376 77% for riverine, and 66% for compound events. On the other hand, no extreme event was indicated by gauge or documentary
377 sources for a small part of the catalogue. The false positive ratio (“E” events to “A”-“D” events) amounts to only 2.2% for
378 compound, 3.3% for coastal, and 5.2% for riverine floods.



379



380

381

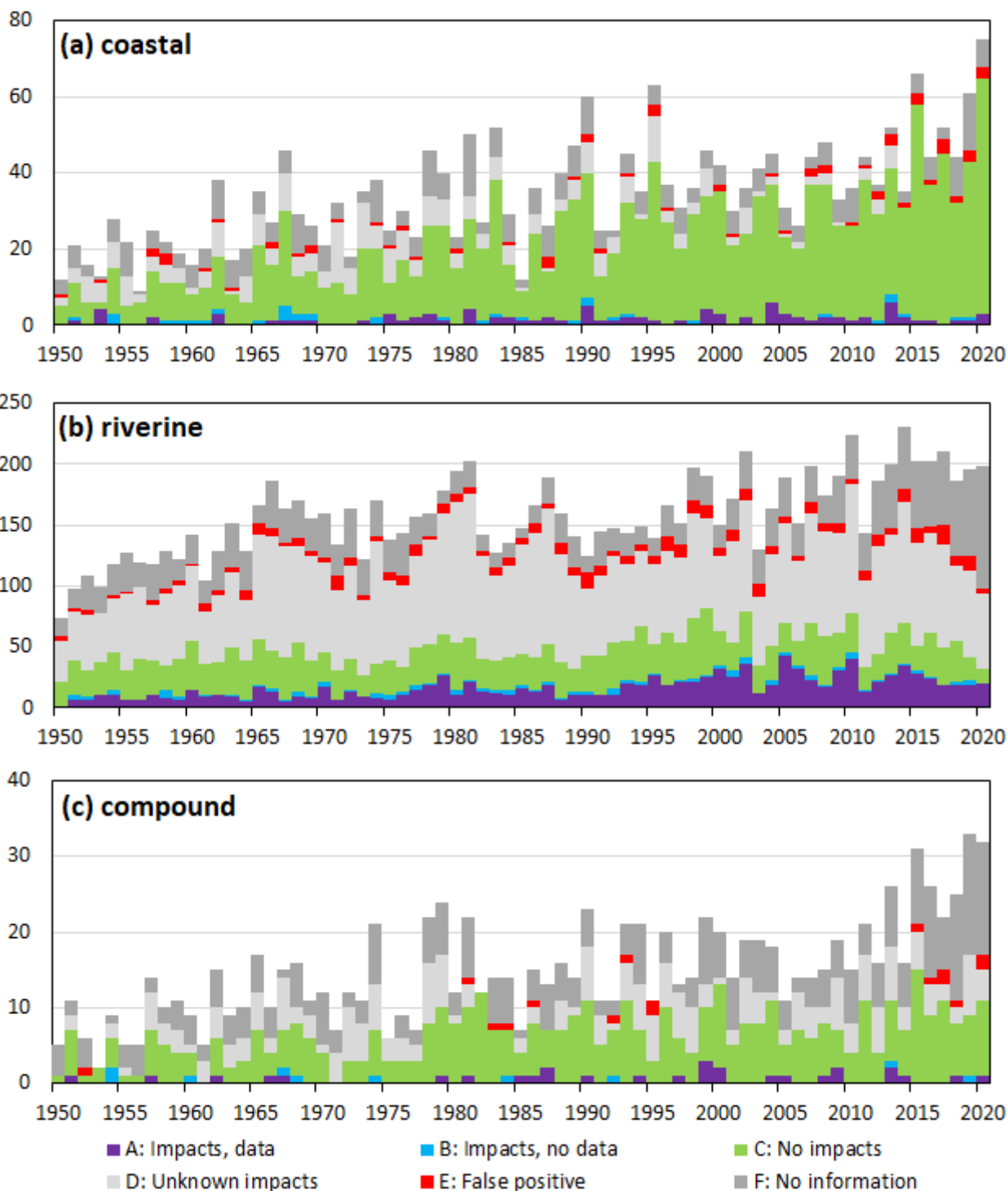
Figure 2. Flood events in the catalogue by classification: (a) coastal, (b) riverine, and (c) compound.

382

383 Confirmation, or at least high confidence based on available documentary sources, whether the event did, or did not, result in
384 significant socioeconomic impacts was possible for the majority of coastal and compound events, but not for riverine floods.
385 However, the latter occurred by far most frequently, and it was possible to confirm significant socioeconomic impacts for
386 11.7% of riverine, 5.4% of coastal, and 3.7% of compound events (Fig. 2). In some cases, “A” (“Impacts, data”) events
387 correspond to more than one reported flood in the HANZE database, or the events are a combination of “A” and “B” (“Impacts,
388 no data”)-type events. Therefore, the 1270 “A” and 207 “B” events actually correspond to 1471 historical floods in HANZE
389 and 237 historical floods without impact data collected in a separate dataset as part of this study (see Appendix A1). This
390 statistic excludes a small number of events that were below the significant impact threshold, but indicated a temporal match
391 with the HANZE database. Only 109 such events were identified, of which only two were coastal events and two were
392 compound events. Out of those, only 33 events, all riverine, were spatially matched with HANZE, a single historical flood in
393 each case. This constitutes only 2% of matched HANZE events, hence we can deem the hydrological and socioeconomic
394 thresholds in this study as well designed, as few HANZE events were missed due to their imposition without creating too many
395 non-impact events. Also, while there were many one-to-many matches between our model and HANZE, largely due to the
396 data-availability rules causing splitting of some flood events in HANZE, there were only a handful of cases of many-to-one
397 connections.

398 The distribution of events over time (Fig. 3) shows an upward trend, which in case of “A” and “B” events is largely related to
399 better availability of data. There is also better confidence in non-occurrence of impacts for coastal and compound events in
400 recent decades compared to the beginning of the timeseries. An increase in “F” events in the final few years for riverine and
401 compound events is primarily connected will lower availability of recent river gauge data.

402



403

404

405

406

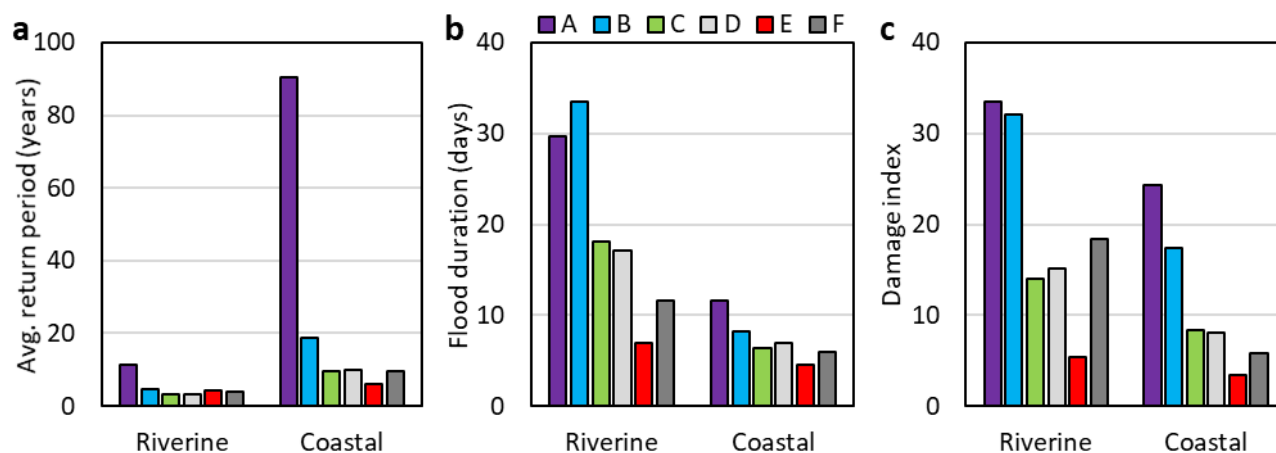
Figure 3. Flood events in the catalogue by year and classification: (a) coastal, (b) riverine, and (c) compound.



407

408 Modelled extremity and impacts of events vary strongly by class (Fig. 4). The return period along affected river and coastal
409 segments is generally much higher for “A” and “B” events compared to all others. 18% of coastal and 37% of riverine events,
410 in which the geometric average of return periods in the affected area was above 25 years, was classified as either “A” or “B”.
411 In contrast, when the return period was below 5 years, the values were 2% and 10%, respectively. Interestingly, the occurrence
412 of “F” class (“No information”) was only slightly lower for higher return periods. Confirmed impactful events were also longer
413 in duration than other classes, with false positives (“E”) having the shortest duration. Consequently, the “A” and “B” events
414 had, on average, the highest impact potential. In Fig. 4c, the dimensionless damage index is the average of four impact
415 categories (potential area inundated, fatalities, persons affected, and economic loss) relative to maximum impact of any event
416 in the country during 1950–2020 at constant 1950 exposure. False positives had, on average, the lowest impact potential. In
417 all examples, the remaining categories (“C” – No impacts, “D” – Unknown impacts, and “F”) oscillated around the average
418 values for all variables analysed in Fig. 4.

419



420

421 **Figure 4. Comparison of mean values of selected indicators by main flood type and classification: (a) average return period along**
422 **affected river or coastal segments, (b) total flood event duration, (c) dimensionless damage index, where 100 equals the highest**
423 **potential impact of any event in the country during 1950–2020 at constant exposure.**

424 3.1.2 Comparison with HANZE reported impacts database

425 The flood catalogue includes the majority of reported historical floods with significant socioeconomic impacts since 1950
426 contained in the HANZE v2.1 database (Paprotny et al., 2023). However, there is a strong difference between the completeness
427 of the catalogue according to flood type. While about 90% of coastal, compound and slow-onset riverine floods were modelled,
428 only 55% of flash floods were captured (Table 5). The latter category, as defined in HANZE, represents short, rapid floods,
429 where the extreme rainfall event triggering the event lasted no more than 24 hours, excluding urban floods. As those often



430 occur in small catchments, they are often not captured as the study was limited only to catchments with an upstream area of at
431 least 100 km².

432 The HANZE database indicates more than 6,000 NUTS3-level impacts since 1950. 78% of those are reproduced by the model
433 (Table 5), a slightly higher percentage than the hit rate at event level (74%). This is largely due to good coverage for slow-
434 onset riverine floods (88%) compared to flash floods (55%), when the former affected more regions on average than the latter.
435 For the 1504 events matched by the model, the hit rate of NUTS3 regions for the model is 89%, again lower for flash floods
436 (84%) than for larger riverine events (91%), not to mention coastal floods (98%). A full list of HANZE events with the
437 information which of those were captured by the model, and which NUTS3 regions were correctly identified is provided
438 together with the dataset on the repository (Paprotny, 2024). In general, performance of the model is stable over time (Fig. 5),
439 though the share of events correctly identified by the model is lower in the very beginning of the model runs (1950s).

440 Analysing the reported impacts in HANZE, even though they are incomplete (except for fatalities), provides further insights.
441 The data in Table 5 show that 97–100% of reported impacts in all four categories for coastal, compound and slow-onset riverine
442 floods were in those historical floods that could also be found in the model. This shows that the model captured almost all
443 large events, and the omissions are mostly minor floods in specific areas where the hazard is apparently not well quantified.
444 For instance, out of 14 omitted coastal and compound floods, 10 are events in Italy occurring mostly before 1964 and affecting
445 200–500 persons with no more than one fatality (with a single exception of a seven-fatality flood from January 1950). Much
446 lower coverage is again for flash floods, as only those responsible for 61% of all fatalities can be found in the model. For other
447 impact categories, the coverage is better, but historical records are very incomplete in relation to those statistics.

448

449

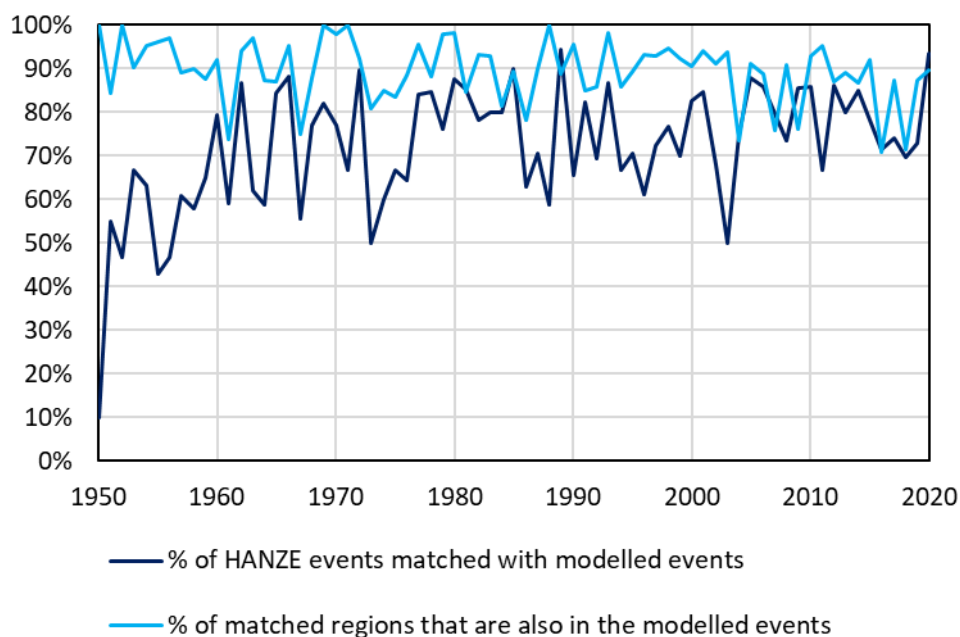


450
 451
 452

Table 5. Comparison of the number of HANZE events, their footprints and reported impacts, with modelled data, 1950–2020. * only regions classified as compound by the model – regions forming compound events in the HANZE database are not necessarily in the zone directly influenced by both riverine and coastal drivers; ** impact data is not available for all HANZE events.

Category	HANZE event type				All events
	Coastal	River/ Coastal	River	Flash	
<i>Matching of events with impact data (“A” events)</i>					
Number of events in HANZE database (1950–2020)	71	41	970	955	2037
Number of modelled events matched with HANZE	61	37	880	526	1504
Percentage of HANZE events matched with modelled events	90%	86%	91%	55%	74%
<i>Matching of affected NUTS3 regions</i>					
Number of affected NUTS3 regions in HANZE database	195	162	4058	1671	6086
Number of affected NUTS3 regions in matched HANZE events	180	152	3910	1084	5326
Number of regions that are also in the modelled events	177	97*	3553	915	4742
Percentage of all regions that are also in the modelled events	91%	60%*	88%	55%	78%
Percentage of matched regions that are also in the modelled events	98%	64%*	91%	84%	89%
<i>Percentage of total reported impacts of all HANZE events within matched HANZE events (1950–2020) **</i>					
Area inundated	99.8%	100%	99.5%	93.2%	99.2%
Fatalities	99.5%	99.4%	97.0%	61.2%	81.2%
Persons affected	99.3%	98.7%	98.9%	78.9%	96.3%
Economic losses in 2020 euros	99.8%	100%	98.9%	86.1%	96.1%
<i>Matching of events without impact data (“B”)</i>					
Number of historical floods without impact data (list B)	27	12	119	79	237

453



454

455

Figure 5. Share of HANZE events matched with the model, and the share of regions in matched events also present in the model.

456

457

3.2 Modelled potential impacts in the flood catalogue

458

Without flood protection measures, floods would have large consequences throughout Europe. A simple summation of flood impacts in the catalogue is not informative, as it assumes not only no flood protection, but also that population and economic activity move into the frequently affected zone in the first place, and then immediately return to previous conditions after each event, even just days after the previous. Considering the total reported impacts in HANZE v2.1, albeit incomplete, it can be estimated that only about 1% of potentially inundated area, population and economic assets were actually affected during 1950–2020. The reported flood deaths equal only about 0.01% of the potential fatalities. Therefore, the potential impacts are merely an intermediate result necessary in the process of estimating flood vulnerability and impact attribution (see section 5). Still, some analysis of the results can be performed as the modelling chain can derive the impact estimates under different exposure scenarios, and it was driven by variable climate conditions.

467

3.2.1 Temporal changes in potential flood impacts

468

For all types of events, an increase in the number of potential events and their impacts was recorded (Table 6). Even though the trends are less pronounced under constant exposure scenarios, they are still equivalent to at least 21% increase in potential coastal flood losses in an average year between 1950 and 2020 in case of fatalities, 47% in case of economic loss and 75% in case of affected population. For riverine floods, the potential impacts have grown even more, while the strongest increase is

471



472 indicated for compound floods, at least threefold since 1950. Potential impacts per flood event are rather similar for coastal
473 and riverine events, and slightly lower for compound events, as the latter category is spatially constrained to regions directly
474 affected by both coastal and riverine drivers.

475 Demographic and economic growth since 1950 has increased potential losses substantially. Presently, exposure of population
476 to riverine floods is more than 50% higher than if population would have not increased, and nearly twice as high for coastal
477 and compound events. Potential impacts relative to the total population in the study area increase more strongly than in the
478 constant-exposure scenario, indicating stronger population growth in areas prone to coastal and compound flooding relative to
479 areas not at risk. However, only a marginal increase in areas at risk of riverine floods was observed relative to areas not prone
480 to this type of floods.

481 Enormous increase in gross domestic product (GDP) per capita (2% per year in the study area), and associated growth in the
482 stock of fixed assets resulted in a five- to six-fold increase in potential losses relative to 1950, and eight- to ten-fold increase
483 in 2020. As the asset growth was higher than GDP, potential economic losses relative to GDP also increased between 1950
484 and 2020. In contrast to population growth, asset growth in flood-prone areas was only marginally higher, or even lower in
485 case of riverine events, than in areas not at risk of flooding.

486
487



488
 489
 490

Table 6. Average potential impacts of floods and their trends, by flood type and exposure scenario (dynamic year-of-event exposure, or fixed at 1950 or 2020 levels). The impacts of compound events mostly overlap with those of coastal and riverine, therefore they should not be added together. Economic losses in constant 2020 prices and exchange rates.

Flood type	Coastal			Riverine			Compound		
	Dyna- mic	1950	2020	Dyna- mic	1950	2020	Dyna- mic	1950	2020
<i>Average potential impacts per year</i>									
Number of events	34	x	x	158	x	x	15	x	x
Area inundated (thsds. km ²)	27	x	x	182	x	x	13	x	x
Fatalities (thousands)	214	133	351	1,059	851	1,246	81	51	108
Persons affected (thousands)	2,689	1,966	3,590	15,284	11,919	18,247	1,004	704	1,239
Economic loss (billion euro)	237	50	478	1,200	261	2,196	86	14	149
<i>Annual increase of potential impacts (%)</i>									
Number of events	1.3	x	x	0.7	x	x	1.5	x	x
Area inundated	1.1	x	x	0.4	x	x	1.6	x	x
Fatalities	1.5	0.4	0.3	1.0	0.6	0.6	2.6	1.6	1.9
Persons affected	1.5	0.9	0.8	1.2	0.8	0.8	2.4	1.7	1.9
Economic loss	2.8	0.6	0.5	3.1	0.9	0.9	4.0	1.8	2.0
<i>Increase in total impacts relative to 1950 exposure</i>									
Fatalities	61%	x	164%	24%	x	46%	59%	x	111%
Persons affected	37%	x	83%	28%	x	53%	43%	x	76%
Economic loss	371%	x	852%	360%	x	742%	505%	x	948%

491

492 3.2.2 Spatial distribution of potential flood impacts

493 Coastal and compound flood potential is highly concentrated in just a few countries (Fig. 6). Though these estimates do not
 494 include the effect of flood protection, the top five countries by coastal flood potential are also most prominently featured in
 495 the HANZE database in terms of historical coastal flood impacts: the Netherlands, the United Kingdom, Germany, France,
 496 and Italy. The same group, plus Ireland, also have the most significant compound flood potential. On the other hand, numerous
 497 potential coastal and compound floods are present in the catalogue for Greece, but only one historical example for that country
 498 could be found in HANZE (a compound flood in 1968 that affected Crete).

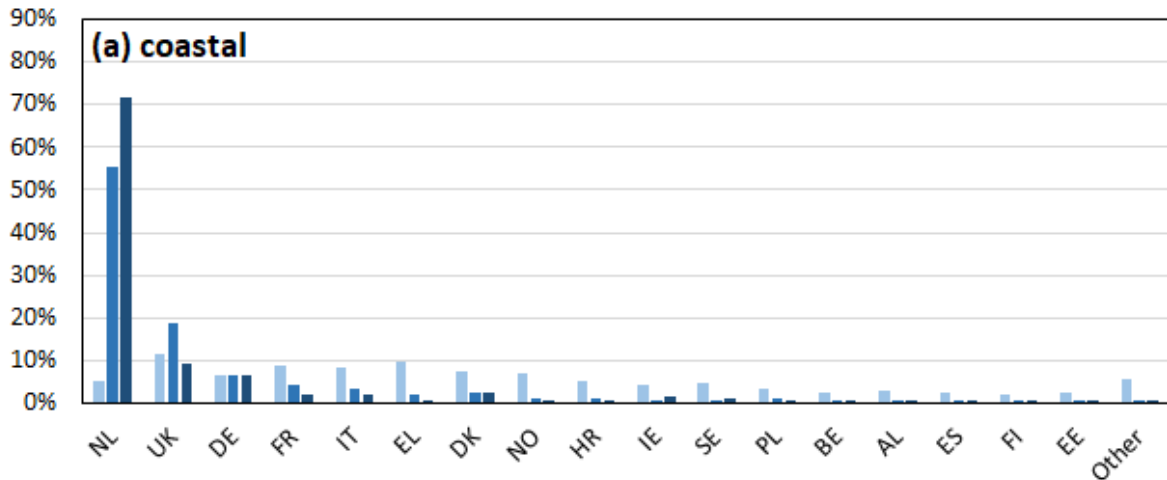
499 In total, the flood catalogue includes coastal floods in 25 countries and compound floods in 24. Slovenia also has no event on
 500 the compound flood list, as none of the compound events was able to pass the higher socioeconomic thresholds for riverine



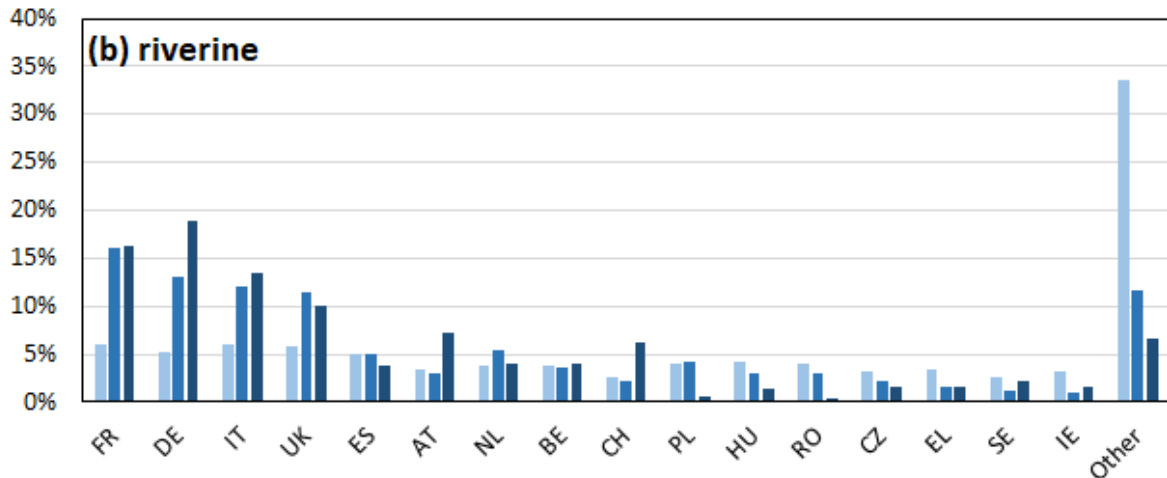
501 and compound events. Bosnia and Herzegovina and Montenegro are the only countries on the compound flood list that are not
 502 present on the coastal flood list due to the limited risk along their short coastlines. Bulgaria is the only country with access to
 503 the sea that is not included in the coastal flood catalogue, as no event exceeded the socioeconomic thresholds. One historical
 504 case of coastal flooding in Bulgaria (in 1999) was recorded in HANZE.

505 Riverine flood potential is more evenly distributed in space. All countries highlighted in Fig. 6b have numerous examples of
 506 historical damaging floods in HANZE, with the exception of the Netherlands, where historical cases are limited to four floods
 507 recorded in the 1990s. In total, 37 out of 42 countries in the study area had at least some potential flood events. Some small
 508 countries had no riverine or compound floods in the catalogue, as they have no river section with an upstream area bigger than
 509 100 km².

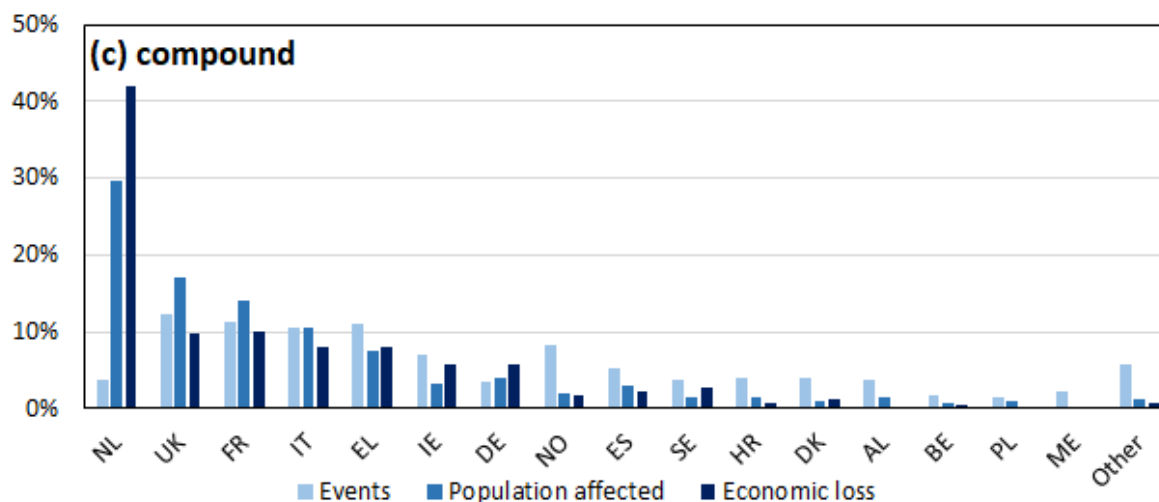
510



511



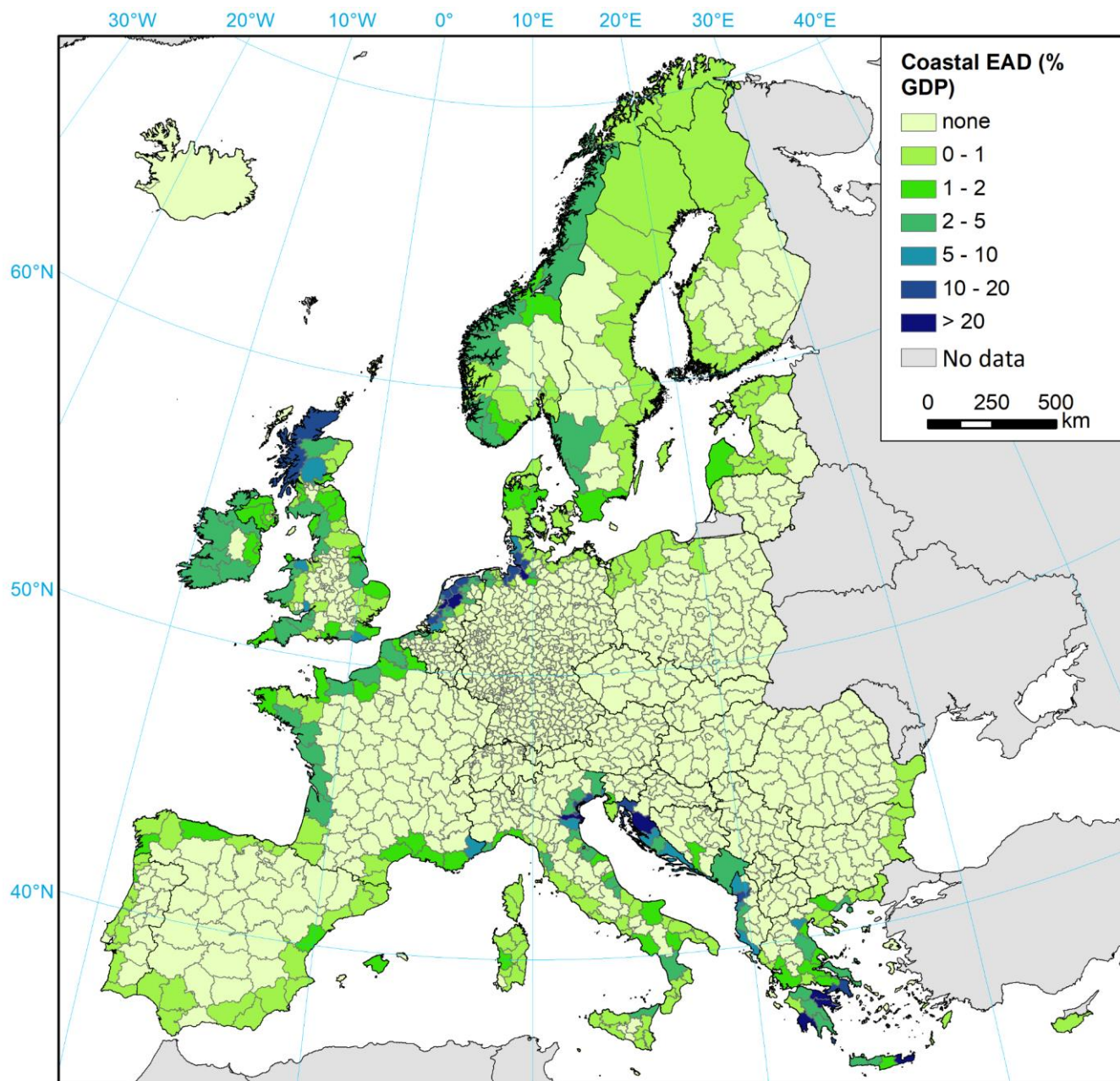
512



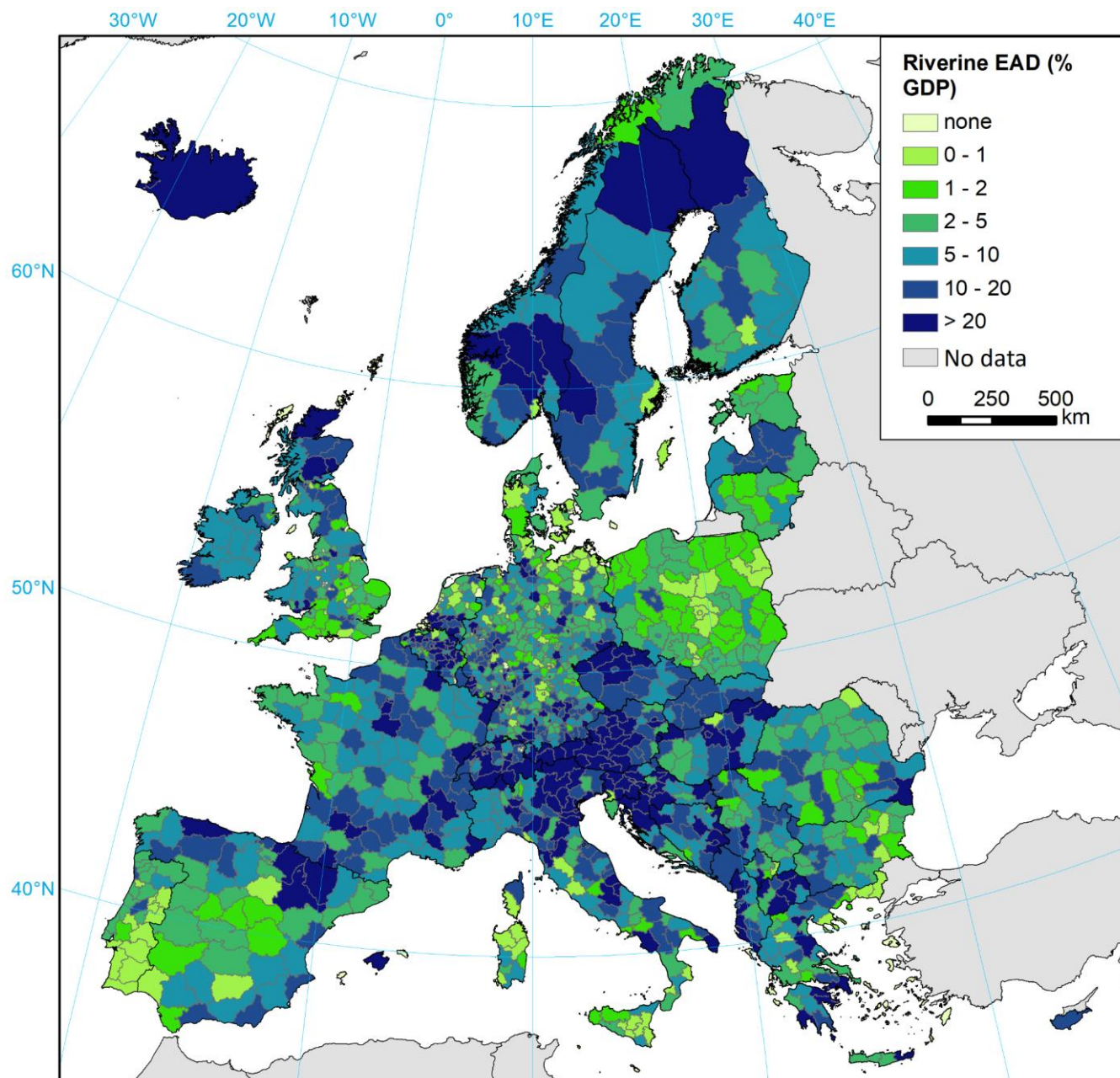
513
514 **Figure 6. Flood events in the catalogue by country and potential impacts, as % of all events: (a) coastal, (b) riverine, and (c)**
515 **compound. Population affected and economic loss in constant 2020 exposure.**

516
517 A variety of indicators can be derived at the level of NUTS3 regions. Here we present one example, potential economic
518 damages normalised to 2020 exposure level, relative to 2020 gross domestic product (GDP). Along most of the European coast
519 potential damages resulting from storm surges are limited (Fig. 7), with risk concentrated along the North Sea, Adriatic Sea,
520 and Aegean Sea. Locations of the most significant past coastal floods stand out (the Netherlands, German Bight, Venice).
521 Riverine damage potential is much higher (Fig. 8), and concentrated around main European mountain ranges (Alps,
522 Carpathians, Pyrenees, Dinaric Alps), as well as Scandinavia and British Isles. Risk is noticeably lower along the Northern
523 European Plain, southwestern Iberian Peninsula, and southern Great Britain. However, it must be stressed that the data
524 represent only damage potential, without considering flood protection or other forms of adaptation.
525 In some parts of Europe, the possibility of co-occurrence of coastal and riverine floods could have large implications on risk.
526 Fig. 9 maps the share of compound flood potential at regional level relative to the total. For each NUTS3 region, we derived a
527 list of all flood events with a potential inundated area of 100 ha, i.e. before aggregation and application of socioeconomic
528 thresholds, then removed riverine and coastal events that overlapped with compound events. In this way, it was possible to
529 avoid double counting and sum together the remaining flood events. The results (Fig. 9) show that compound potential is very
530 unevenly distributed across Europe. In northern and eastern coasts of the Adriatic Sea, Greece, Ireland, western and southern
531 coasts of Great Britain, and certain parts of France, Italy, Spain, and Norway, compound events could potentially contribute
532 20–25% or even more of all economic losses from flooding. In all aforementioned countries there are known examples of
533 damaging floods contained in the HANZE database.

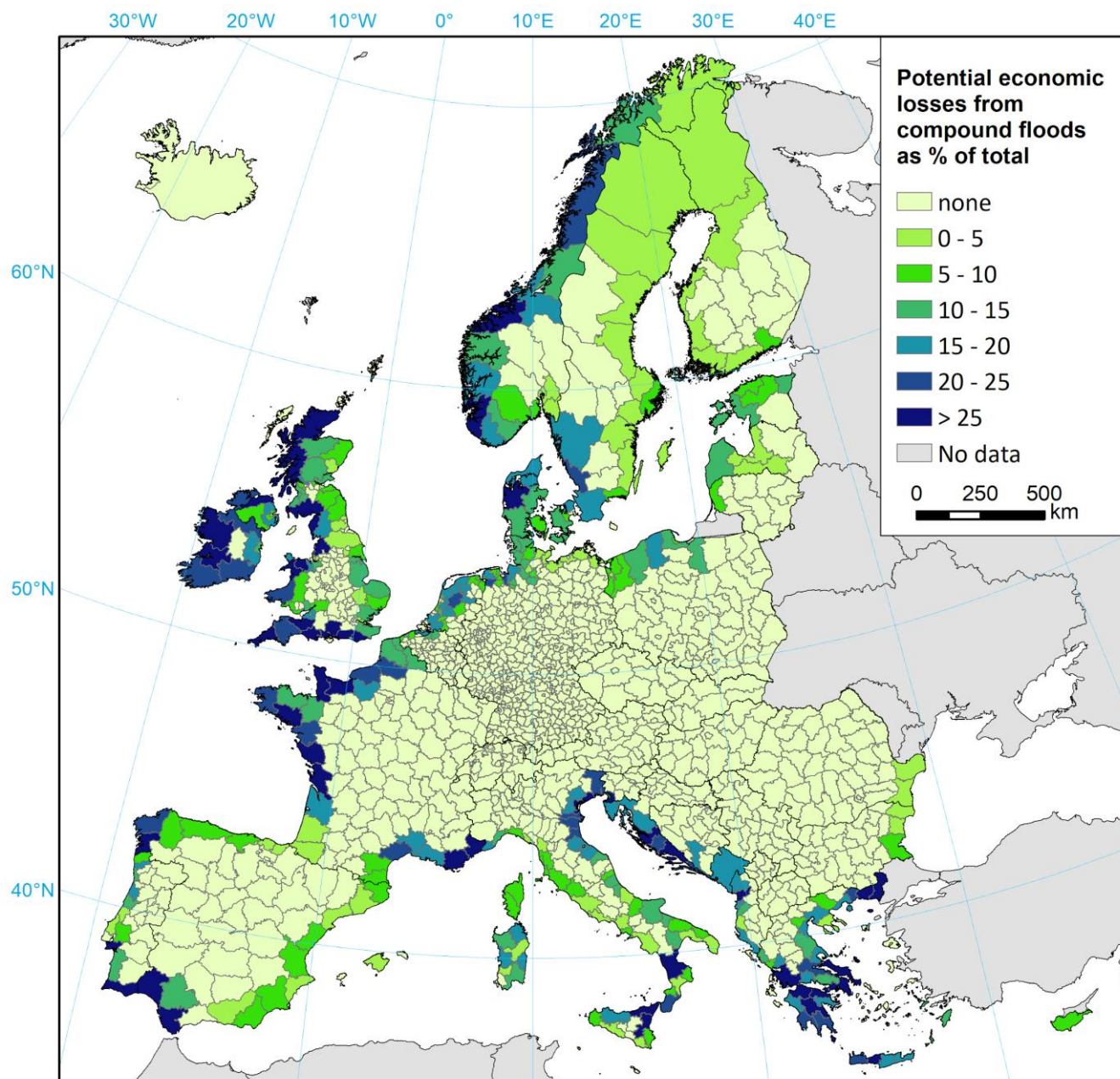
534



535
536 **Figure 7. Potential expected annual economic damage of coastal floods as % of GDP, 1950–2020, in constant 2020 exposure, per**
537 **NUTS3 region. Potential impacts per region include all events above 100 ha flooded area threshold per NUTS3 region, including**
538 **those not passing the socioeconomic impact thresholds.**



539
540 **Figure 8. Potential expected annual economic damage of riverine floods as % of GDP, 1950–2020, in constant 2020 exposure, per**
541 **NUTS3 region. Potential impacts per region include all events above 100 ha flooded area threshold per NUTS3 region, including**
542 **those not passing the socioeconomic impact thresholds.**



543

544 **Figure 9. Share of compound floods is total potential economic losses, 1950–2020, in constant 2020 exposure, per NUTS3 region.**
545 **Potential impacts per region include all events above 100 ha flooded area threshold per NUTS3 region, including those not passing**
546 **the socioeconomic impact thresholds. Individual riverine and coastal events contributing to compound events were excluded to**
547 **compute this metric.**



548 **3.3 Validation**

549 **3.3.1 Extreme river discharges**

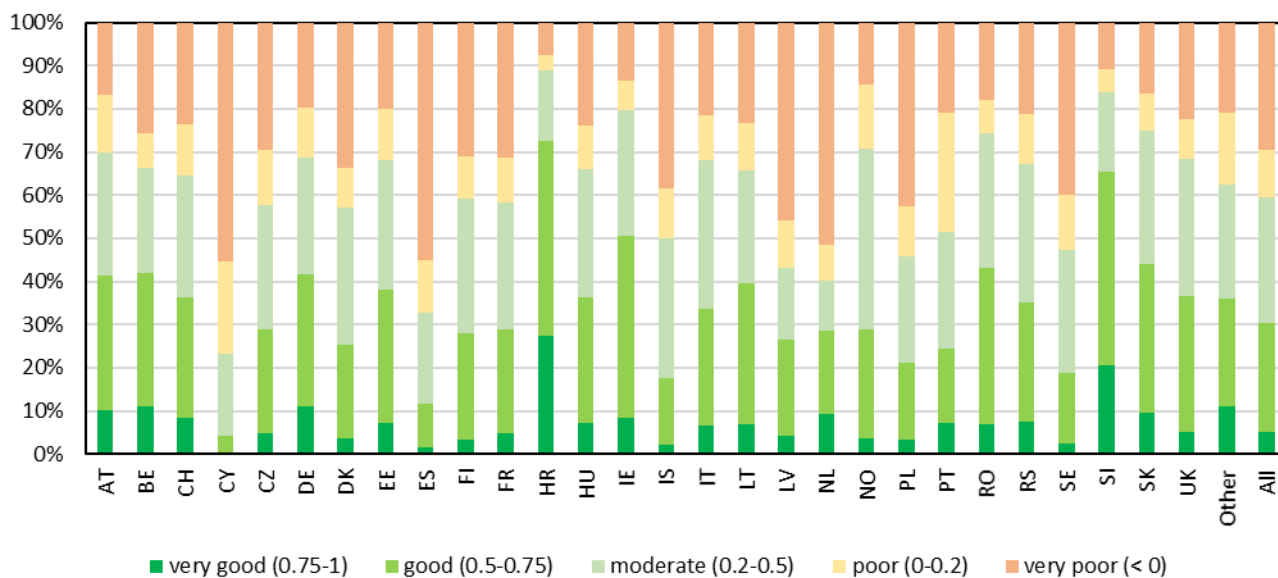
550 At least one river discharge station with adequate data length was available for 7742 events (63% of the total), and nearly
551 292,000 timeseries were identified within the NUTS3 regions potentially affected by those events. Most of the data is available
552 for events that have occurred in the United Kingdom, Poland, Spain, Sweden, Germany, France, and Norway. The R^2 between
553 modelled and observed peak discharge for all event time series, standardised by reported upstream area, is 0.45. However, the
554 relative discharges are more of interest of this study, and modelled peak discharges corrected for difference in average annual
555 discharges have an R^2 of 0.63. The timeseries of daily discharge during the events is good (0.5-0.75) or very good (0.75-1) for
556 59% of all station-events in terms of Spearman's R^2 , and for 30% in terms of KGE score. On the other hand, poor (0-0.2) or
557 very poor (<0) performance was recorded for 18% and 41% of stations, respectively. There is relatively little difference in
558 performance depending on classification of events, except for far worse results for events classified as false positives ("E").
559 Here, the poor or very poor score was recorded for 83% of station-events, compared to 37% for HANZE flood events ("A").
560 Performance also varies strongly by location (Fig. 10), with e.g. Germany, Ireland, Austria, Belgium, and Slovakia recording
561 much higher shares of good or very good station performance (above 40%) than e.g. Poland, Spain, Sweden, and Portugal (less
562 than 25%).

563

564

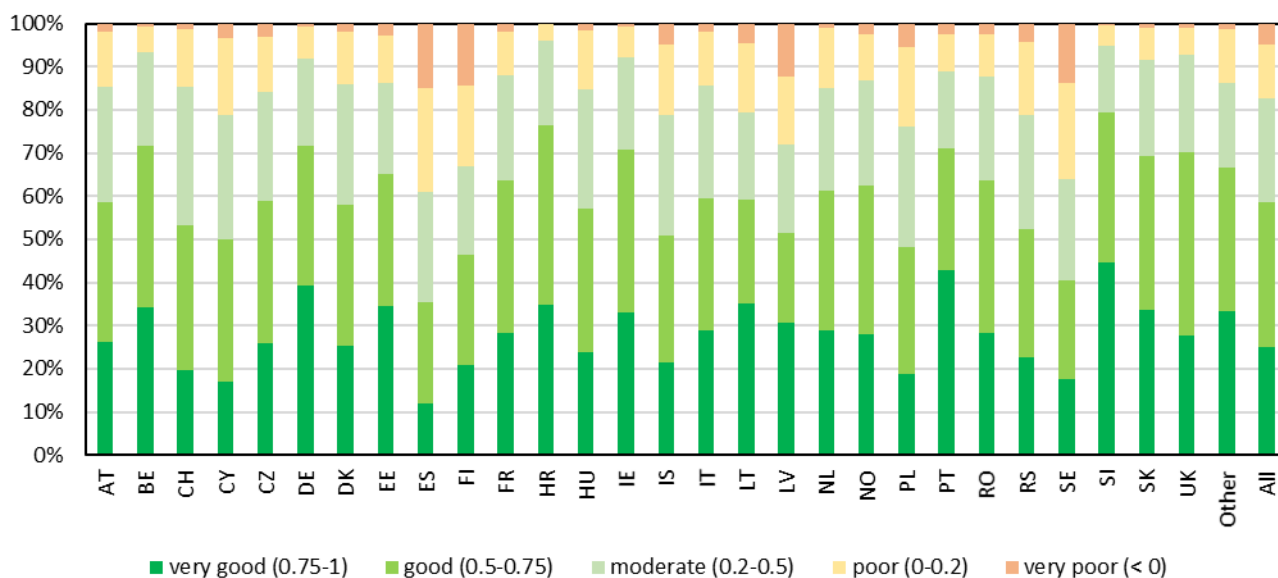


a



565

b



566

567 **Figure 10. Comparison of daily river discharge during flood events in the catalogue, or a 30-day window centred around the dates**
 568 **of the event. Abbreviations are NUTS level 0 country codes. The graph shows the percentage of all stations per country by**
 569 **performance class: (a) KGE score; (b) Spearman's coefficient of determination.**



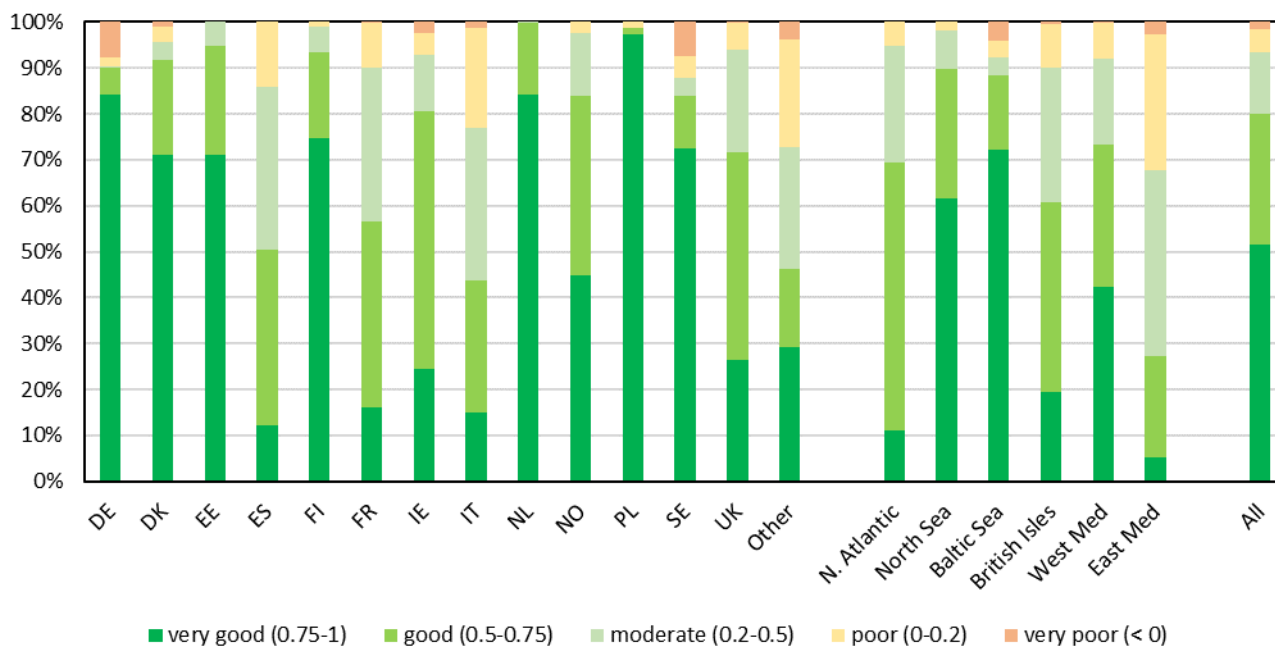
570 **3.3.2 Extreme sea levels**

571 At least one tide gauge with adequate data length was available for 1363 events (56% of the total), and a total of 8102 time
572 series were identified within the NUTS3 regions potentially affected by those events. Most of the data is available for events
573 that have occurred in the United Kingdom, Denmark, Norway, the Netherlands, France, Sweden, and Germany. The overall
574 results are compared using several metrics in Table 7. Overall, the maximum sea levels observed during the various potential
575 coastal floods were well reproduced, with the main source of inaccuracies being storm surge heights. Further, 80% of modelled
576 time series spanning the duration of the events indicated a good or very good R^2 when compared with observations. For tides
577 and total water level, such performance was measured for 93–94% of stations. The best performance of the storm surge model
578 was recorded for North and Baltic seas (Fig. 11), with far lower performance for the Eastern Mediterranean Sea. However,
579 potential flood events and observational data are both relatively scarce in the latter region, which had the lowest scores also
580 for reproducing tides and combined sea level. As in the case of riverine events, there is little variation between events by
581 classification, though historical HANZE events (“A”) had slightly higher scores for storm surge heights and combined sea
582 level than all other classes. This could be, to some extent, the result of the difference in the geographical distribution of events.

583
584 **Table 7. Comparison between maximum hourly sea level and its components during flood events in the catalogue, or a 7-day window**
585 **centred around the dates of the event.**

Metric	Storm surge height	Tide elevation	Combined sea level
Pearson’s R^2	0.75	0.99	0.96
Spearman’s R^2	0.74	0.95	0.94
Nash-Sutcliffe Efficiency	0.47	0.99	0.96
Root mean squared error (RMSE) in metres	0.30	0.14	0.26
RMSE to standard deviation ratio	0.53	0.11	0.21

586



587

588 **Figure 11. Comparison between maximum hourly storm surge height during flood events in the catalogue, or a 7-day window centred**
 589 **around the dates of the event. The graph shows the percentage of all stations per country by performance of Pearson's R^2 .**
 590 **Abbreviations in the left side of the graph are NUTS level 0 country codes. On the right side of the graph, stations are grouped by**
 591 **main European sea regions: "N. Atlantic" – exposed North Atlantic Ocean coasts (mostly France and Spain), "North Sea" – including**
 592 **Norwegian coasts, "Baltic Sea" – including Danish Straits, "British Isles" – coasts of Great Britain and Ireland, "West Med" and**
 593 **"East Med" – Western and Eastern Mediterranean Sea, respectively.**

594 3.3.3 Flood footprints

595 Comparison of modelled potential flood impacts with impacts based on satellite-derived flood footprints and actual impacts
 596 recorded in the HANZE database highlights the challenge of correctly recreating past floods (Table 8). For exactly half of the
 597 20 floods for which a satellite-derived footprint is available, our modelled population affected were closer to reported
 598 population affected than estimates based on satellite-derived flood footprints, and vice versa. In most cases, satellite-derived
 599 footprints severely underestimated the extent of the flooding, with the exception of floods in the United Kingdom, where they
 600 indicated many times more affected population than the reported actual impact. In all cases the modelled area and persons
 601 affected were higher than the actual impact, as was the intention of the catalogue, as modelled without flood protection.
 602 However, there is a very close match in persons affected during the August 2002 flood in Czechia and Germany. In the whole
 603 catalogue, the area affected was higher than reported in 83% of cases where the actual impact was reported in HANZE (i.e.
 604 256 out of 307), fatalities in 98% of cases (1473 out of 1496), population affected in 89% of cases (686 out of 773) and
 605 economic loss in 89% of cases (675 out of 755).

606



607
608
609

Table 8. Comparison of modelled potential flood zone with satellite-derived footprints from the Global Flood Database (Tellman et al., 2021) and reported impacts from HANZE (Paprotny et al., 2023) for several European floods, 2002–2015. Area flooded in km². * percentage of the satellite flood footprint reproduced by the modelled flood footprint of this study.

Event (country, month, year)	HANZE ID	Reported impacts (HANZE)		Modelled impacts with potential flood zone		Modelled impacts with satellite footprints		Hit rate modelled area to satellite area*	Ratio of affected population	
		Area flooded	Persons affected	Area flooded	Persons affected	Area flooded	Persons affected		Modelled: reported	Reported: satellite
Albania, November/December 2010	2031	139	24,700	894	91,776	194	8,260	56%	3.7	3.0
Austria, March 2006	21		1,840	263	15,130	68	1,659	45%	8.2	1.1
Bosnia and Herzegovina, April-May 2004	2053	200	20,000	734	147,114	75	1,023	44%	7.4	19.6
Czechia, August 2002	86		225,000	1247	225,513	90	4,018	54%	1.0	56.0
France, September 2002	244		12,000	763	116,813	95	1,595	30%	9.7	7.5
France, December 2003	250		27,000	1,843	245,870	767	11,954	67%	9.1	2.3
Germany, August 2002	341		330,000	3,371	372,649	681	10,081	74%	1.1	32.7
Greece, January/February 2015	403	250	500	405	3,696	268	256	44%	7.4	2.0
Hungary, March-May 2006	421	2,440	5,400	5,201	310,750	918	10,886	37%	57.5	0.5
Hungary, May/June 2010	422	1,230	5,000	1,376	77,306	199	214	85%	15.5	23.3
Italy, November/December 2002	952		10,000	2,031	424,594	119	29,321	13%	42.5	2.9
Italy, January 2003	954		40,000	370	43,917	35	392	18%	1.1	102.0
Lithuania, March/April 2010	2200	400	2,000	1,211	27,851	214	464	59%	13.9	4.3
Montenegro, December 2010	2209		6,630	289	21,390	198	2,330	34%	3.2	2.8
Poland, May/June 2010	1065	5,540	280,000	7,151	775,536	348	9,757	71%	2.8	28.7
Romania, July 2005	1148	993	58,700	1,664	85,918	338	1,061	50%	1.5	55.3
Romania, April/May 2006	1153	1,165	15,011	5,305	115,330	3,415	6,626	43%	7.7	2.3
UK, November/December 2012	1558		4,400	1,156	132,320	869	265,903	12%	30.1	0.02
UK, December 2013-February 2014	1561	450	25,000	828	225,781	815	388,930	13%	9.0	0.06
UK, December 2015-January 2016	1563		64,000	1,016	100,633	1,472	480,026	9%	1.6	0.13

610

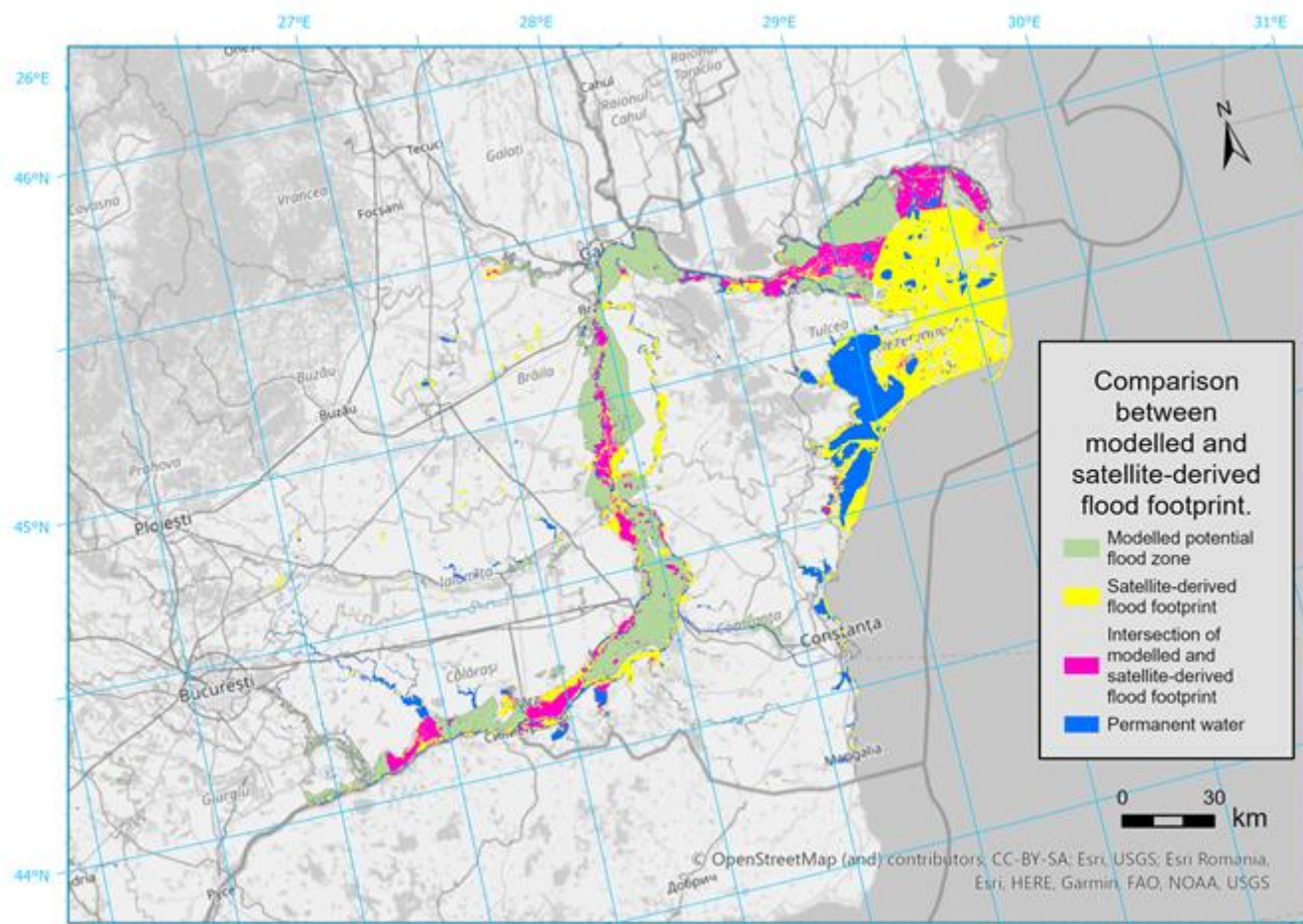
611

612

Direct comparison between modelled and satellite footprints (Fig. 12) has shown that the hit rate, i.e. share of the satellite footprints correctly reproduced by the model, varied between 30 and 85%, except for events in Italy and the United Kingdom,



613 where it was only 9–18%. However, the satellite footprints also performed very poorly against reported losses for those floods.
614 Some additional flood events were analysed, but were not included in Table 6 as the satellite footprints showed virtually no
615 population affected, which is in large contrast to actual impacts. Such a situation occurred e.g. for the summer floods in the
616 United Kingdom in 2007 that flooded homes of about 192,000 people (HANZE database number 1546), almost none of which
617 could be reproduced with satellite flood footprints.
618



619
620 **Figure 12. Example comparison between modelled and satellite-derived flood footprint of the 2006 event in Romania.**

621 **4 Discussion**

622 **4.1 Uncertainties and limitations of the models and modelled data**

623 The elaborate modelling chain involving both riverine and coastal processes is subject to multiple cascading limitations and
624 uncertainties. The starting point of the simulations are input climate data, derived from global reanalyses. Though ERA5 and



625 ERA5-Land are state-of-the-art, they still encounter problems of inhomogeneities, gaps or errors in observational data, model
626 biases, and limitations in representing precipitation extremes in particular (Hersbach et al., 2020, Muñoz-Sabater et al., 2021).
627 In the case of the riverine model, bias-adjustment and downscaling was carried out, but it is also only a statistical transformation
628 that depends on the quality of high-resolution observations as well (see section 4.1.2).
629 Validation results in section 3.1 indicate mostly good performance of the models in reconstructing past extreme discharges
630 and sea levels, but not in all areas. Some regions are more challenging to model than others, e.g. due to complex topography
631 or shoreline, or strong anthropogenic influence on the water cycle (especially through reservoirs). Not all types of floods or
632 processes that drive them could be represented. Most noticeably, the resolution of the riverine model is inadequate to capture
633 smaller flash floods, as the hydrological model has a spatial resolution of 1' driven by climate data that was twice downscaled
634 (first from ERA5 to ERA5-Land, then using ISIMIP3BASD method) and with a temporal resolution of six hours. Additionally,
635 flood hazard maps used to generate the footprints only covered catchments with an upstream area of at least 100 km².
636 Consequently, 91% of slow-onset riverine floods from HANZE were reproduced, but only 55% of flash floods. Urban floods
637 are not represented at all (also in the HANZE dataset).
638 Further, no flood defences are represented in the model, which is by design, as information on this aspect is scarce, especially
639 in the temporal dimension. At the same time, a flood that was historically prevented by existing defences might not have been
640 prevented under counterfactual conditions. We also hypothesise that flood protection levels are driven to some extent by flood
641 risk and flood occurrence (section 4.2). The use of flood hazard maps for a defined set of scenarios enables generating flood
642 footprints without carrying out a computationally infeasible continuous hydrodynamic simulation over a period of 71 years.
643 However, the maps assume a specific hydrograph which is not necessarily valid for all floods with the same peak discharge.
644 Further, the three sets of maps (including two sets for different catchment sizes) are methodologically different and were
645 created for diverse sets of scenarios. Whereas the coastal maps were rerun specifically for this study based on the results of
646 the extreme sea level modelling, the riverine maps are from previous studies. Their application is in some locations problematic
647 due to inconsistencies in river network delineation between EFAS and the hazard maps. The accuracy of the riverine flood
648 hazard maps is also variable depending on the region and the probability of occurrence (see Paprotny et al., 2017, and Dottori
649 et al., 2022, for details).
650 Compound floods are represented by merging riverine and coastal flood zones, which neglects the possible interaction between
651 the storm surge and river discharge that could generate higher water levels than is possible for individual drivers. Additionally,
652 not all coastal processes are included in the model, such as interaction between tide and storm surges, or influence of SLR on
653 tide elevations. Wave run-up is only approximated by taking one-fifth of offshore significant wave height, as more precise
654 estimates would require a very detailed model of the nearshore. Finally, long-term land motion is limited to GIA due to lack
655 of detailed data on the subject.



656 **4.2 Uncertainties and limitations of the observations and documentary sources**

657 The results are influenced not only by the accuracy of models, but also that of the observations. Our river discharge simulations
658 are driven by reanalysis data that were downscaled and bias-adjusted using interpolated meteorological observations, the
659 accuracy of which depends strongly on the density of point meteorological data. As shown in Thiemig et al. (2022),
660 precipitation during extreme events in the EMO dataset can at times diverge strongly from other reported measurements.
661 Though our meteorological input data is still driven primarily by ERA5, the reanalysis itself is influenced by availability of
662 meteorological data, which is very inhomogeneous in time (Hersbach et al., 2020). This might be the reason for the noticeably
663 lower performance of our model in reproducing flood events in the 1950s.

664 Model calibration and validation, as well as classification of the flood event catalogue is affected by the availability of tide
665 and river gauges (section 3.1.1 and 3.1.2). The data is unevenly distributed, with most data available for northern Europe,
666 particularly the Nordic countries and the British Isles. On the other hand, very limited data was available for Italy, Greece, and
667 Balkan countries. It is further uneven in time, with both the 1950s and the last few years until 2020 having lower coverage
668 than the 1990s and 2000s in particular. Identification of events as false positives (“E”) is also potentially problematic, as in
669 large NUTS3 regions the only available observations could be outside the impact zone of the event, hence incorrectly
670 suggesting that the model generated a ‘bogus’ event. Satellite-derived footprints were used to validate the modelled flood
671 footprints, but themselves often widely diverged from reported impacts. The hit rate between satellite and model data varied
672 significantly between individual events, similarly observed in a reconstruction of recent European coastal floods by Le Gal et
673 al. (2023).

674 Similarly, documentary sources on socioeconomic impacts of floods are highly uneven in quality between countries. For
675 instance, while there are comprehensive databases and flood catalogues accessible e.g. for France, Italy, Norway, Portugal,
676 Spain, or Switzerland, and even some Balkan countries, scattering of information makes it very laborious to collect data for
677 other countries, e.g. Austria, Germany, and the United Kingdom. Many compilations of flood impacts only cover the recent
678 two decades, while older flood catalogues published in the 1980s or 1990s often have no newer follow-ups. This strongly
679 affects the frequency of “C” (No impacts) events relative to “D” (Impacts unknown). Thanks to extensive research in the
680 HANZE database, this has less effect on detection of “A” (Impacts, data) and “B” (Impacts, no data) events. Still, uncertainty
681 surrounds designation of flood events as having “significant” socioeconomic impacts. The thresholds defined in HANZE are
682 somewhat arbitrary, though based on experience of collecting more than 2500 records in the dataset. In case of smaller events,
683 their classification is uncertain if the data is incomplete or not very accurate. This is potentially problematic for “B” events,
684 where at times no quantitative data at all is available, and the classification was based on the description of impacts only.
685 Finally, NUTS3 regions, the principal socioeconomic unit of observation here and in HANZE, vary in size both in terms of
686 area and population. It might be slightly easier for floods in large regions to pass region-scale threshold for minimum flood
687 area in the model, and to be considered affected in HANZE, where region-scale impact thresholds are also applied when
688 detailed damage data are available.



689 **5 Conclusions**

690 This study is the largest attempt to reconstruct past flood losses in Europe, and makes an advance towards full decomposition
691 of drivers of historical flood losses. We created a flood catalogue for Europe containing 14,699 events with significant
692 socioeconomic impact potential. It covers riverine, coastal and compound events over a period of 71 years, and considers
693 climate change, evolving human impact on catchments, and growing exposure. The catalogue includes 1504 out of 2037
694 damaging floods since 1950 included in HANZE dataset (Paprotny et al., 2023), including some 90% of coastal, compound
695 and slow-onset riverine floods, and 55% of flash floods. The coverage of reported impacts of those events is 81-99% depending
696 on the exact measure. The performance of the model is relatively stable over time, though slightly worse for the 1950s.

697 The flood catalogue was primarily devised as the baseline (factual) reconstruction of past floods in Europe. However, it can
698 be also used directly for multiple applications. The immediate follow-up to this analysis will be modelling changes in flood
699 preparedness in Europe in the past 70 years, including flood protection standards and relative losses (vulnerability). The
700 modelling chain can be further used with counterfactual climate inputs. Methods such as ATTRICI (Mengel et al., 2021) enable
701 removing the global warming effect from all variables required to model riverine discharges. Additional counterfactual
702 simulations are possible to quantify the human influence on catchments, particularly through construction of reservoirs
703 (Boulangé et al., 2021). Methods such as transformed-stationary extreme value analysis (Mentaschi et al., 2016) can be used
704 to detrend storm surge heights in addition to removing the long-term sea level rise. Together with HANZE historical exposure
705 maps (Paprotny and Mengel, 2023), counterfactual scenarios for all components of risk would be achieved. This would provide
706 the first comprehensive impact attribution of European flood losses and generate an important reference dataset for pan-
707 European flood risk assessments.

708
709 *Data & code availability:* Numerous public datasets and models were used in the study, results of which are also publicly
710 available. Details were to find each dataset and model are provided in Appendix A3.

711 *Author contributions.* DP developed the concept, implemented the methods, collected and processed most of the data, and
712 acquired funding. BR collected part of the historical impact data and performed part of the flood event classification. MV
713 computed coastal flood hazard maps. PT and JS performed the validation based on satellite-derived flood footprints and created
714 the online visualisation of the study. FD and ST contributed datasets and methods for the riverine and coastal simulations,
715 respectively. LF and HK helped to develop the concept and methods. All authors wrote the paper.

716 *Competing interests.* The authors declare that they have no conflict of interest.

717 *Financial support.* This research has been supported by the German Research Foundation (DFG) through project
718 “Decomposition of flood losses by environmental and economic drivers” (FloodDrivers), grant no. 449175973.



719 **Appendix A1. Contents of “B” list of historical floods**

720 The format of the database of “B” list events follows the same format of HANZE database (Paprotny et al., 2023), with a
 721 reduced number of fields as events were confined to the “B” list specifically due to lack of relevant data (primarily flood
 722 impact statistics). Most fields have strictly-defined permitted values, except “Notes”, which includes explanation why impacts
 723 should be considered significant (using partial available data or descriptive indicators), and “Data sources” which lists all cited
 724 references. The latter are often the same as used in the HANZE database, therefore only publications specific to the B list are
 725 included in the full bibliographic details provided with the event file. For detailed discussion about the contents of each field
 726 we refer to Paprotny et al. (2023).

727
 728 **Table A1. Summary of fields recorded in the “B” list of floods.**

Variable	Short description	Field type	Permitted values
ID	Unique event identifier	integer	7000...8999
Country code	Two-letter country code	string	Codes from Table B1
Year	Year of the event	integer	1950...2020
Country name	Country name	string	Names from Table B1
Start date	Daily start date	date	1.1.1950...31.12.2020
End date	Daily end date	date	1.1.1950...31.01.2021
Type	Detailed type of event	string	River, Flash, Coastal, River/Coastal
Regions affected (NUTS3 v2010)	Regions where human or economic losses were reported, at NUTS3 level (version 2010)	string	Codes from Table B2
Regions affected (NUTS3 v2021)	As above, but at using NUTS version 2021	string	Codes from Table B3
Notes	Other relevant information or notes on issues with the data	string	Free text
References	List of publications and databases from which the information was obtained	string	Free text

729
 730



731 **Appendix A2. Contents of the modelled flood event catalogue**

732 **Table A2. Summary of fields recorded in the modelled flood event catalogue.**

Variable	Short description
ID	Unique event identifier
Country code	Two-letter country code
Year	Year of the event
Country name	Country name
Start date	Daily start date
End date	Daily end date
Type	Detailed type of event
Flood source	Rivers or sea basins in the potentially-affected area (from Vogt et al., 2007, and Fourcy and Lorvelec, 2013)
Regions affected (NUTS3 v2010)	Regions where human or economic losses were reported, at NUTS3 level (version 2010)
Regions affected (NUTS3 v2021)	As above, but at using NUTS version 2021
Area inundated	Potential inundated area in hectares (ha)
Fatalities, YE	Potential fatalities, in persons, year-of-event exposure
Fatalities, 1950	Potential fatalities, in persons, 1950 exposure
Fatalities, 2020	Potential fatalities, in persons, 2020 exposure
Persons affected, YE	Potential persons affected, in persons, year-of-event exposure
Persons affected, 1950	Potential persons affected, in persons, 1950 exposure
Persons affected, 2020	Potential persons affected, in persons, 2020 exposure
Economic loss, YE	Potential direct economic loss, in thousands of 2020 euros, year-of-event exposure
Economic loss, 1950	Potential direct economic loss, in thousands of 2020 euros, 1950 exposure
Economic loss, 2020	Potential direct economic loss, in thousands of 2020 euros, 2020 exposure
Loss threshold	Threshold for direct economic losses applied to the event, in thousands of 2020 euros
Mean water depth	Average water depth in the potential inundated zone
Return period	Average (geometric) of return periods along potential affected river grid cells or coastal segments, from detrended 1950–2020 data, Generalised Pareto distribution
Hydro data	Indicates if river or tide gauge data were available for this event (1 – yes, 0 – no)
RP2 exceedance	Indicates if a 2-year return period was exceeded in the observational data (1 – yes, 0 – no)
Category	Classification of event according to Table 4
HANZE ID	Flood event ID if event classified as “A” or “B”, otherwise empty field

733

734



735 **Appendix A3. Availability of data and models**

736 **Table A3. Availability of input and output data and models from the study. Models are indicated by *italics*.**

Variable, data	Dataset/ <i>model</i>	Resource link
River discharges	HERA	https://data.jrc.ec.europa.eu/dataset/a605a675-9444-4017-8b34-d66be5b18c95
Meteorological data for storm surge simulation, significant wave height	ERA5	https://doi.org/10.24381/cds.e2161bac
<i>Hydrodynamic model (coastal)</i>	<i>Delft3D</i>	https://oss.deltares.nl/web/delft3d/get-started
Tide elevation constituents	FES2014	https://www.aviso.altimetry.fr/en/data/products/auxiliary-products/global-tide-fes.html
<i>Tide elevation model</i>	<i>pyTMD</i>	https://github.com/tsutterley/pyTMD
Mean dynamic topography	Global Ocean Mean Dynamic Topography	https://doi.org/10.48670/moi-00150
Sea level rise	Hourly Coastal water levels with Counterfactual	https://zenodo.org/records/7771386
Sea level rise	European Seas Gridded L 4 Sea Surface Heights	https://doi.org/10.48670/moi-00141
Sea level rise	Global Ocean Gridded L 4 Sea Surface Heights	https://doi.org/10.48670/moi-00148
Glacial isostatic adjustment	ICE-6G_C	https://www.atmosph.physics.utoronto.ca/~peltier/data.php
Storm surge heights, combined water level, tide levels	This study	https://doi.org/10.5281/zenodo.10630338
DEM for coastal inundation	GLO-30	https://doi.org/10.5069/G9028PQB
<i>Hydrodynamic model for coastal inundation</i>	<i>Lisflood-ACC</i>	https://www.seamlesswave.com/LISFLOOD8.0
Land use and population at 100 m resolution	HANZE v2.0 output maps	https://doi.org/10.5281/zenodo.7885990
<i>Exposure model (population, fixed assets by sector)</i>	<i>HANZE v2.0</i>	https://doi.org/10.5281/zenodo.7556953
Historical flood impacts (“A” list) and list of references	HANZE v2.1	https://doi.org/10.5281/zenodo.8410025
Significant flood events without direct impact data (“B” list)	This study	https://doi.org/10.5281/zenodo.10629443
List of documentary sources used	This study	https://doi.org/10.5281/zenodo.10629443
Coastal flood hazard maps, flood catalogue input data	This study	https://doi.org/10.5281/zenodo.10630862
River flood hazard maps	JRC maps	https://doi.org/10.2905/1D128B6C-A4EE-4858-9E34-6210707F3C81
River flood hazard maps	RAIN project maps	https://doi.org/10.4121/uuid:968098ce-afe1-4b21-a509-dedaf9bf4bd5
Historical flood database	EM-DAT	https://public.emdat.be/
Historical flood database	EEA Flood Phenomena	https://www.eea.europa.eu/data-and-maps/data/european-past-floods/flood-phenomena
Historical flood database	Dartmouth Flood Observatory	http://floodobservatory.colorado.edu/Archives/index.html
Historical flood database	FFEM-DB	https://doi.org/10.4121/14754999.v2
Historical flood database	Recorded Flood Outlines	https://www.data.gov.uk/dataset/16e32c53-35a6-4d54-a111-ca09031eaaaf/recorded-flood-outlines
River discharge data	GRDC	https://portal.grdc.bafg.de/
River discharge data (France)	HydroPortail	https://www.hydro.eaufrance.fr/rechercher/entites-hydrometriques



River discharge data (Norway)	NVE, Historiske vannføringsdata til produksjonsplanlegging	https://www.nve.no/vann-og-vassdrag/hydrologiske-data/historiske-data/historiske-vannfoeringsdata-til-produksjonsplanlegging/
River discharge data (Spain)	Centro de Estudios Hidrográficos, Anuario de aforos	https://ceh.cedex.es/anuarioaforos/default.asp
River discharge data (Sweden)	SMHI Vattenweb	https://www.smhi.se/data/hydrologi/vattenwebb
River discharge data (UK)	UK National River Flow Archive	https://nrfa.ceh.ac.uk/
River discharge, sea level data (Poland)	IMGW-PIB, Dane Publiczne	https://danepubliczne.imgw.pl/
Sea level data	GESLA v3	https://gesla787883612.wordpress.com/
Sea level data	Poseidon System	https://poseidon.hcmr.gr/services/ocean-data/situ-data
Satellite flood footprints	Global Flood Database	https://global-flood-database.cloudtostreet.ai/#interactive-map
<i>Flood catalogue generation model</i>	<i>This study</i>	https://doi.org/10.5281/zenodo.10678820
Modelled flood catalogue	This study	https://doi.org/10.5281/zenodo.10629443
Modelled flood footprints	This study	https://doi.org/10.5281/zenodo.10640692

737

738 References

- 739 Argus, D.F., Peltier, W.R., Drummond, R., and Moore, A.W.: The Antarctica component of postglacial rebound model ICE-
 740 6G_C (VM5a) based upon GPS positioning, exposure age dating of ice thicknesses, and relative sea level histories, *Geophys.*
 741 *J. Int.*, 198, 537-563, <https://doi.org/10.1093/gji/ggu140>, 2014.
- 742 Arnal, L., Asp, S.-S., Baugh, C., de Roo, A., Disperati, J., Dottori, F., Garcia, R., Garcia Padilla, M., Gelati, E., Gomes, G.,
 743 Kalas, M., Krzeminski, B., Latini, M., Lorini, V., Mazzetti, C., Mikulickova, M., Muraro, D., Prudhomme, C., Rauthe-Schöch,
 744 A., Rehfeldt, K., Salamon, P., Schweim, C., Skoien, J. O., Smith, P., Sprokkereef, E., Thiemig, V., Wetterhall, F., and Ziese,
 745 M.: EFAS upgrade for the extended model domain – technical documentation, Publications Office of the European Union,
 746 Luxembourg, <https://doi.org/10.2760/806324>, 2019.
- 747 Bates, P. D., Horritt, M. S., and Fewtrell, T. J.: A simple inertial formulation of the shallow water equations for efficient two-
 748 dimensional flood inundation modelling, *J. Hydrol.*, 387, 33–45, <https://doi.org/10.1016/j.jhydrol.2010.03.027>, 2010.
- 749 Batista e Silva, F., Lavalle, C., and Koomen, E.: A procedure to obtain a refined European land use/cover map, *J. Land Use*
 750 *Sci.*, 8, 255–283, <https://doi.org/10.1080/1747423X.2012.667450>, 2012.
- 751 Bednar-Friedl, B., Biesbroek, R., Schmidt, D.N., Alexander, P., Børshiem, K. Y., Carnicer, J., Georgopoulou, E., Haasnoot,
 752 M., Le Cozannet, G., Lionello, P., Lipka, O., Möllmann, C., Muccione, V., Mustonen, T., Piepenburg, D., and Whitmarsh, L.:
 753 Europe, *Climate Change 2022: Impacts, Adaptation and Vulnerability*, Contribution of Working Group II to the Sixth
 754 Assessment Report of the Intergovernmental Panel on Climate Change, Cambridge University Press, Cambridge, UK and New
 755 York, NY, USA, 1817–1927, <https://doi.org/10.1017/9781009325844.015>, 2022.



- 756 Blöschl, G., Kiss, A., Viglione, A., Barriendos, M., Böhm, O., Brázdil, R., Coeur, D., Demarée, G., Llasat, M. C., Macdonald,
757 N., Retsö, D., Roald, L., Schmocker-Fackel, P., Amorim, I., Belinová, M., Benito, G., Bertolin, C., Camuffo, D., Cornel, D.,
758 Doctor, R., Elleder, L., Enzi, S., Garcia, J. C., Glaser, R., Hall, J., Haslinger, K., Hofstätter, M., Komma, J., Limanówka, D.,
759 Lun, D., Panin, A., Parajka, J., Petric, H., Rodrigo, F. S., Rohr, C., Schönbein, J., Schulte, L., Silva, L. P., Toonen, W., Valent,
760 P., Waser, J., and Wetter, O.: Current flood-rich period is exceptional compared to the past 500 years in Europe, *Nature*, 583,
761 560–566, <https://doi.org/10.1038/s41586-020-2478-3>, 2020.
- 762 Boulange, J., Hanasaki, N., Yamazaki, D., and Pokhrel, Y.: Role of dams in reducing global flood exposure under climate
763 change, *Nat Commun.*, 12, 417, <https://doi.org/10.1038/s41467-020-20704-0>, 2021.
- 764 Boyd, E., Levitan, M., and van Heerden, I.: Further specification of the dose-response relationship for flood fatality estimation,
765 paper presented at the US-Bangladesh workshop on innovation in windstorm/storm surge mitigation construction, National
766 Science Foundation and Ministry of Disaster & Relief, Government of Bangladesh, Dhaka, 19–21 December 2005.
- 767 Brakenridge, G. R.: Global Active Archive of Large Flood Events. Dartmouth Flood Observatory, University of Colorado,
768 available at <http://floodobservatory.colorado.edu/Archives/index.html> (last access: 26 October 2023), 2023.
- 769 Burek, P., van der Knijff, J., and De Roo, A.: LISFLOOD - Distributed Water Balance and Flood Simulation Model - Revised
770 User Manual 2013, Publications Office of the European Union, Luxembourg, <https://doi.org/10.2788/24982>, 2013.
- 771 Centre for Research on the Epidemiology of Disasters: EM-DAT, CRED / UCLouvain, Brussels, Belgium,
772 <https://www.emdat.be/> (last access: 26 October 2023), 2023.
- 773 Choulga, M., Moschini, F., Mazzetti, C., Grimaldi, S., Disperati, J., Beck, H., Salamon, P., and Prudhomme, C.: Technical
774 note: Surface fields for global environmental modelling, *EGUsphere* [preprint], <https://doi.org/10.5194/egusphere-2023-1306>,
775 2023.
- 776 Copernicus Emergency Management Service: European Flood Awareness System (EFAS) version 5.0, available at
777 <https://confluence.ecmwf.int/display/CEMS/European+Flood+Awareness+System> (last access: 8 November 2023), 2023.
- 778 Diederer, D., Liu, Y., Gouldby, B., Diermanse, F., and Vorogushyn, S.: Stochastic generation of spatially coherent river
779 discharge peaks for continental event-based flood risk assessment, *Nat. Hazards Earth Syst. Sci.*, 19, 1041–1053,
780 <https://doi.org/10.5194/nhess-19-1041-2019>, 2019.
- 781 Dottori, F., Alfieri, L., Bianchi, A., Skoien, J., and Salamon, P.: A new dataset of river flood hazard maps for Europe and the
782 Mediterranean Basin, *Earth Syst. Sci. Data*, 14, 1549–1569, <https://doi.org/10.5194/essd-14-1549-2022>, 2022.
- 783 Enríquez, A. R., Wahl, T., Marcos, M., and Haigh, I. D.: Spatial footprints of storm surges along the global coastlines, *J.*
784 *Geophys. Res.-Oceans*, 125, e2020JC016367, <https://doi.org/10.1029/2020JC016367>, 2020.
- 785 Environment Agency: Recorded Flood Outlines, available at [https://www.data.gov.uk/dataset/16e32c53-35a6-4d54-a111-](https://www.data.gov.uk/dataset/16e32c53-35a6-4d54-a111-ca09031eaaaf/recorded-flood-outlines)
786 [ca09031eaaaf/recorded-flood-outlines](https://www.data.gov.uk/dataset/16e32c53-35a6-4d54-a111-ca09031eaaaf/recorded-flood-outlines) (last access: 31 October 2023), 2023.
- 787 European Environment Agency: Flood phenomena, available at [https://www.eea.europa.eu/data-and-maps/data/european-](https://www.eea.europa.eu/data-and-maps/data/european-past-floods/flood-phenomena)
788 [past-floods/flood-phenomena](https://www.eea.europa.eu/data-and-maps/data/european-past-floods/flood-phenomena) (last access: 26 October 2023), 2015.



- 789 European Space Agency and Sinergise: Copernicus Global Digital Elevation Model, OpenTopography [dataset],
790 <https://doi.org/10.5069/G9028PQB>, 2021.
- 791 Eurostat: Statistical regions in the European Union and partner countries NUTS and statistical regions 2021 - re-edition 2022,
792 Publications Office of the European Union, Luxembourg, <https://doi.org/10.2785/321792>, 2022.
- 793 Fourcy, D., and Lorvelec, O.: A new digital map of limits of oceans and seas consistent with high-resolution global shorelines,
794 *J. Coast. Res.*, 29, 471–477, <http://dx.doi.org/10.2112/JCOASTRES-D-12-00079.1>, 2013.
- 795 Frieler, K., Volkholz, J., Lange, S., Schewe, J., Mengel, M., del Rocio Rivas López, M., Otto, C., Reyer, C. P. O., Karger, D.
796 N., Malle, J. T., Treu, S., Menz, C., Blanchard, J. L., Harrison, C. S., Petrik, C. M., Eddy, T. D., Ortega-Cisneros, K., Novaglio,
797 C., Rousseau, Y., Watson, R. A., Stock, C., Liu, X., Heneghan, R., Tittensor, D., Maury, O., Büchner, M., Vogt, T., Wang, T.,
798 Sun, F., Sauer, I. J., Koch, J., Vanderkelen, I., Jägermeyr, J., Müller, C., Rabin, S., Klar, J., Vega del Valle, I. D., Lasslop, G.,
799 Chadburn, S., Burke, E., Gallego-Sala, A., Smith, N., Chang, J., Hantson, S., Burton, C., Gädeke, A., Li, F., Gosling, S. N.,
800 Müller Schmied, H., Hattermann, F., Wang, J., Yao, F., Hickler, T., Marcé, R., Pierson, D., Thiery, W., Mercado-Bettín, D.,
801 Ladwig, R., Ayala-Zamora, A. I., Forrest, M., and Bechtold, M.: Scenario setup and forcing data for impact model evaluation
802 and impact attribution within the third round of the Inter-Sectoral Model Intercomparison Project (ISIMIP3a), *Geosci. Model*
803 *Dev.*, 17, 1–51, <https://doi.org/10.5194/gmd-17-1-2024>, 2024.
- 804 Ganguli, P., Paprotny, D., Hasan, M., Güntner, A., Merz, B.: Projected changes in compound flood hazard from riverine and
805 coastal floods in Northwestern Europe, *Earth's Future*, 8, e2020EF001752, <https://doi.org/10.1029/2020EF001752>, 2020.
- 806 Haigh, I. D., Marcos, M., Talke, S. A., Woodworth, P. L., Hunter, J. R., and Hague, B. S.: GESLA Version 3: A major update
807 to the global higher-frequency sea-level dataset, *Geosci. Data J.*, 10, 293–314, <https://doi.org/10.1002/gdj3.174>, 2023.
- 808 Hersbach, H., Bell, B., Berrisford, P., et al.: The ERA5 global reanalysis, *Q. J. R. Meteorol. Soc.*, 146, 1999–2049,
809 <https://doi.org/10.1002/qj.3803>, 2020.
- 810 Huizinga, J., de Moel, H., Szweczyk, W.: Global flood depth-damage functions. Methodology and the database with
811 guidelines, Publications Office of the European Union, Luxembourg, <https://doi.org/10.2760/16510>, 2017.
- 812 Institute of Meteorology and Water Management – National Research Institute: Dane publiczne. Available at:
813 <https://danepubliczne.imgw.pl/> (last access: 11 November 2023), 2023.
- 814 Jacob, D., Petersen, J., Eggert, B. et al.: EURO-CORDEX: new high-resolution climate change projections for European
815 impact research, *Reg. Environ. Change*, 14, 563–578, <https://doi.org/10.1007/s10113-013-0499-2>, 2014.
- 816 Jones, P. W.: First- and Second-Order Conservative Remapping Schemes for Grids in Spherical Coordinates, *Mon. Weather*
817 *Rev.*, 127, 2204–2210, [https://doi.org/10.1175/1520-0493\(1999\)127<2204:FASOCR>2.0.CO;2](https://doi.org/10.1175/1520-0493(1999)127<2204:FASOCR>2.0.CO;2), 1999.
- 818 Jonkman, S. N., Vrijling, J. K., and Vrouwenvelder, A. C. W. M.: Methods for the estimation of loss of life due to floods: a
819 literature review and a proposal for a new method, *Nat. Hazards*, 46, 353–389, <https://doi.org/10.1007/s11069-008-9227-5>,
820 2008.
- 821 Klein Goldewijk, K., Beusen, A., Doelman, J., and Stehfest, E.: Anthropogenic land use estimates for the Holocene – HYDE
822 3.2, *Earth Syst. Sci. Data*, 9, 927–953, <https://doi.org/10.5194/essd-9-927-2017>, 2017.



- 823 Kreibich, H., Blauhut, V., Aerts, J. C. J. H., Bouwer, L. M., Van Lanen, H. A. J., Mejia, A., Mens, M., and Van Loon, A. F.:
824 How to improve attribution of changes in drought and flood impacts, *Hydrolog. Sci. J.*, 64, 1–18,
825 <https://doi.org/10.1080/02626667.2018.1558367>, 2019.
- 826 Kreibich, H., Schröter, K., Di Baldassarre, G., Van Loon, A. F., Mazzoleni, M., Abeshu, G. W., Agafonova, S., AghaKouchak,
827 A., Aksoy, H., Alvarez-Garreton, C., Aznar, B., Balkhi, L., Barendrecht, M. H., Biancamaria, S., Bos-Burginger, L., Bradley,
828 C., Budiyo, Y., Buytaert, W., Capewell, L., Carlson, H., Cavus, Y., Couasnon, A., Coxon, G., Daliakopoulos, I., de Ruiter,
829 M. C., Delus, C., Erfurt, M., Esposito, G., François, D., Frappart, F., Freer, J., Frolova, N., Gain, A. K., Grillakis, M., Grima,
830 J. O., Guzmán, D. A., Huning, L. S., Ionita, M., Kharlamov, M., Khoi, D. N., Kieboom, N., Kireeva, M., Koutroulis, A.,
831 Lavado-Casimiro, W., Li, H.-Y., Llasat, M. C., Macdonald, D., Mård, J., Mathew-Richards, H., McKenzie, A., Mejia, A.,
832 Mendiondo, E. M., Mens, M., Mobini, S., Mohor, G. S., Nagavciuc, V., Ngo-Duc, T., Nguyen, H. T. T., Nhi, P. T. T., Petrucci,
833 O., Quan, N. H., Quintana-Seguí, P., Razavi, S., Ridolfi, E., Riegel, J., Sadik, M. S., Sairam, N., Savelli, E., Sazonov, A.,
834 Sharma, S., Sörensen, J., Souza, F. A. A., Stahl, K., Steinhausen, M., Stoelzle, M., Szalińska, W., Tang, Q., Tian, F.,
835 Tokarczyk, T., Tovar, C., Tran, T. V. T., van Huijgevoort, M. H. J., van Vliet, M. T. H., Vorogushyn, S., Wagener, T., Wang,
836 Y., Wendt, D. E., Wickham, E., Yang, L., Zambrano-Bigiarini, M., and Ward, P. J.: Panta Rhei benchmark dataset: socio-
837 hydrological data of paired events of floods and droughts, *Earth Syst. Sci. Data*, 15, 2009–2023, [https://doi.org/10.5194/essd-](https://doi.org/10.5194/essd-15-2009-2023)
838 [15-2009-2023](https://doi.org/10.5194/essd-15-2009-2023), 2023.
- 839 Kreibich, H., Van Loon, A. F., Schröter, K., Ward, P. J., Mazzoleni, M., Sairam, N., Abeshu, G. W., Agafonova, S.,
840 AghaKouchak, A., Aksoy, H., Alvarez-Garreton, C., Aznar, B., Balkhi, L., Barendrecht, M. H., Biancamaria, S., Bos-
841 Burgering, L., Bradley, C., Budiyo, Y., Buytaert, W., Capewell, L., Carlson, H., Cavus, Y., Couasnon, A., Coxon, G.,
842 Daliakopoulos, I., de Ruiter, M. C., Delus, C., Erfurt, M., Esposito, G., François, D., Frappart, F., Freer, J., Frolova, N., Gain,
843 A. K., Grillakis, M., Grima, J. O., Guzmán, D. A., Huning, L. S., Ionita, M., Kharlamov, M., Khoi, D. N., Kieboom, N.,
844 Kireeva, M., Koutroulis, A., Lavado-Casimiro, W., Li, H., Llasat, M. C., Macdonald, D., Mård, J., Mathew-Richards, H.,
845 McKenzie, A., Mejia, A., Mendiondo, E. M., Mens, M., Mobini, S., Mohor, G. S., Nagavciuc, V., Ngo-Duc, T., Nguyen, H.
846 T. T., Nhi, P. T. T., Petrucci, O., Quan, N. H., Quintana-Seguí, P., Razavi, S., Ridolfi, E., Riegel, J., Sadik, M. S., Savelli, E.,
847 Sazonov, A., Sharma, S., Sörensen, J., Souza, F. A. A., Stahl, K., Steinhausen, M., Stoelzle, M., Szalińska, W., Tang, Q., Tian,
848 F., Tokarczyk, T., Tovar, C., Tran, T. V. T., Van Huijgevoort, M. H. J., van Vliet, M. T. H., Vorogushyn, S., Wagener, T.,
849 Wang, Y., Wendt, D. E., Wickham, E., Yang, L., Zambrano-Bigiarini, M., Blöschl, G., and Di Baldassarre, G.: The challenge
850 of unprecedented floods and droughts in risk management, *Nature*, 608, 80–86, <https://doi.org/10.1038/s41586-022-04917-5>,
851 2022.
- 852 Lange, S.: Trend-preserving bias adjustment and statistical downscaling with ISIMIP3BASD (v1.0), *Geosci. Model Dev.*, 12,
853 3055–3070, <https://doi.org/10.5194/gmd-12-3055-2019>, 2019.
- 854 Lange, S.: ISIMIP3BASD (3.0.0), Zenodo [code], <https://doi.org/10.5281/zenodo.6501284>, 2022.



- 855 Le Gal, M., Fernández-Montblanc, T., Duo, E., Montes Perez, J., Cabrita, P., Souto Ceccon, P., Gastal, V., Ciavola, P., and
856 Armaroli, C.: A new European coastal flood database for low–medium intensity events, *Nat. Hazards Earth Syst. Sci.*, 23,
857 3585–3602, <https://doi.org/10.5194/nhess-23-3585-2023>, 2023.
- 858 Lehner, B., Reidy Liermann, C., Revenga, C., Vörösmarty, C., Fekete, B., Crouzet, P., Döll, P., Endejan, M., Frenken, K.,
859 Magome, J., Nilsson, C., Robertson, J. C., Rodel, R., Sindorf, N., and Wisser, D.: High-resolution mapping of the world’s
860 reservoirs and dams for sustainable river-flow management, *Front. Ecol. Environ.*, 9, 494–502, <https://doi.org/10.1890/100125>,
861 2011.
- 862 Lyard, F. H., Allain, D. J., Cancet, M., Carrère, L., and Picot, N.: FES2014 global ocean tide atlas: design and performance,
863 *Ocean Sci.*, 17, 615–649, <https://doi.org/10.5194/os-17-615-2021>, 2021.
- 864 Mengel, M., Treu, S., Lange, S., and Frieler, K.: ATTRICI v1.1 – counterfactual climate for impact attribution, *Geosci. Model*
865 *Dev.*, 14, 5269–5284, <https://doi.org/10.5194/gmd-14-5269-2021>, 2021.
- 866 Mentaschi, L., Voudoukas, M., Voukouvalas, E., Sartini, L., Feyen, L., Besio, G., and Alfieri, L.: The transformed-stationary
867 approach: a generic and simplified methodology for non-stationary extreme value analysis, *Hydrol. Earth Syst. Sci.*, 20, 3527–
868 3547, <https://doi.org/10.5194/hess-20-3527-2016>, 2016.
- 869 Merz, B., Blöschl, G., Vorogushyn, S., Dottori, F., Aerts, J. C., Bates, P., Bertola, M., Kemter, M., Kreibich, H., and Lall, U.:
870 Causes, impacts and patterns of disastrous river floods, *Nature Reviews Earth & Environment*, 2, 592–609,
871 <https://doi.org/10.1038/s43017-021-00195-3>, 2021.
- 872 Mester, B., Frieler, K., and Schewe, J.: Human displacements, fatalities, and economic damages linked to remotely observed
873 floods, *Sci. Data*, 10, 482, <https://doi.org/10.1038/s41597-023-02376-9>, 2023.
- 874 Muis, S., Apecechea, M. I., Dullaart, J., de Lima Rego, J., Madsen, K. S., Su, J., Yan, K., and Verlaan, M.: A High-resolution
875 global dataset of extreme sea levels, tides, and storm surges, including future projections, *Frontiers in Marine Science*, 7, 263,
876 <https://doi.org/10.3389/fmars.2020.00263>, 2020.
- 877 Mulet, S., Rio, M.-H., Etienne, H., Artana, C., Cancet, M., Dibarboure, G., Feng, H., Husson, R., Picot, N., Provost, C., and
878 Strub, P. T.: The new CNES-CLS18 global mean dynamic topography, *Ocean Sci.*, 17, 789–808, <https://doi.org/10.5194/os-17-789-2021>, 2021.
- 880 Muñoz-Sabater, J., Dutra, E., Agustí-Panareda, A., Albergel, C., Arduini, G., Balsamo, G., Boussetta, S., Choulga, M.,
881 Harrigan, S., Hersbach, H., Martens, B., Miralles, D. G., Piles, M., Rodríguez-Fernández, N. J., Zsoter, E., Buontempo, C.,
882 and Thépaut, J.-N.: ERA5-Land: a state-of-the-art global reanalysis dataset for land applications, *Earth Syst. Sci. Data*, 13,
883 4349–4383, <https://doi.org/10.5194/essd-13-4349-2021>, 2021.
- 884 Nicholls, R. J., Lincke, D., Hinkel, J., Brown, S., Vafeidis, A. T., Meyssignac, B., Hanson, S. E., Merkens, J. L., and Fang, J.:
885 A global analysis of subsidence, relative sea-level change and coastal flood exposure, *Nat. Clim. Change*, 11, 338–342,
886 <https://doi.org/10.1038/s41558-021-00993-z>, 2021.
- 887 Papagiannaki, K., Petrucci, O., Diakakis, M., Kotroni, V., Aceto, L., Bianchi, C., Brázdil, R., Gelabert, M. G., Inbar, M.,
888 Kahraman, A., Kılıç, Ö., Krahn, A., Kreibich, H., Llasat, M. C., Llasat-Botija, M., Macdonald, N., de Brito, M. M., Mercuri,



- 889 M., Pereira, S., Řehoř, J., Geli, J. R., Salvati, P., Vinet, F., Zêzere, J. L.: Developing a large-scale dataset of flood fatalities for
890 territories in the Euro-Mediterranean region, *FFEM-DB, Sci. Data*, 9, 166, <https://doi.org/10.1038/s41597-022-01273-x>, 2022.
- 891 Paprotny, D. and Morales-Nápoles, O.: Estimating extreme river discharges in Europe through a Bayesian network, *Hydrol.*
892 *Earth Syst. Sci.*, 21, 2615–2636, doi:10.5194/hess-21-2615-2017, 2017
- 893 Paprotny, D., Mengel, M.: Population, land use and economic exposure estimates for Europe at 100 m resolution from 1870
894 to 2020, *Sci. Data*, 10, 372, <https://doi.org/10.1038/s41597-023-02282-0>, 2023.
- 895 Paprotny, D., Morales Nápoles, O., Nikulin, G.: Extreme sea levels under present and future climate: a pan-European database,
896 *E3S Web of Conferences*, 7, 02001, <https://doi.org/10.1051/e3sconf/20160702001>, 2016.
- 897 Paprotny, D., Morales Nápoles, O., Vousdoukas, M. I., Jonkman, S. N., and Nikulin, G.: Accuracy of pan-European coastal
898 flood mapping, *J. Flood Risk Manag.*, 12(2), e12459, <https://doi.org/10.1111/jfr3.12459>, 2019.
- 899 Paprotny, D., Morales-Nápoles, O., and Jonkman, S. N.: Efficient pan-European river flood hazard modelling through a
900 combination of statistical and physical models, *Nat. Hazards Earth Syst. Sci.*, 17, 1267–1283, [https://doi.org/10.5194/nhess-](https://doi.org/10.5194/nhess-17-1267-2017)
901 [17-1267-2017](https://doi.org/10.5194/nhess-17-1267-2017), 2017.
- 902 Paprotny, D., Morales-Nápoles, O., and Jonkman, S. N.: HANZE: a pan-European database of exposure to natural hazards and
903 damaging historical floods since 1870, *Earth Syst. Sci. Data*, 10, 565–581, <https://doi.org/10.5194/essd-10-565-2018>, 2018a.
- 904 Paprotny, D., Sebastian, A., Morales Nápoles, O., and Jonkman, S. N.: Trends in flood losses in Europe over the past 150
905 years, *Nat. Commun.*, 9, 1985, <https://doi.org/10.1038/s41467-018-04253-1>, 2018b.
- 906 Paprotny, D., Terefenko, P., and Śledziowski, J.: An improved database of flood impacts in Europe, 1870–2020: HANZE v2.1,
907 *Earth Syst. Sci. Data Discuss.* [preprint], <https://doi.org/10.5194/essd-2023-321>, in review, 2023.
- 908 Paprotny, D.: HANZE catalogue of modelled and historical floods in Europe, 1950-2020 [dataset],
909 <https://doi.org/10.5281/zenodo.10629443>, 2024.
- 910 Peltier, W.R., Argus, D.F., and Drummond, R.: Space geodesy constrains ice-age terminal deglaciation: The global ICE-6G_C
911 (VM5a) model, *J. Geophys. Res. Solid Earth*, 120, 450–487, <https://doi.org/10.1002/2014JB011176>, 2015.
- 912 Poseidon System: Monitoring, forecasting and information system for the Greek seas, available at <https://poseidon.hcmr.gr/>.
913 Last accessed 16 January 2024.
- 914 Pronk, M.: DeltaDTM: A global coastal digital terrain model. Version 1 [dataset], <https://doi.org/10.4121/21997565.v1>, 2023.
- 915 Pujol, M.-I., Faugère, Y., Taburet, G., Dupuy, S., Pelloquin, C., Ablain, M., and Picot, N.: DUACS DT2014: the new multi-
916 mission altimeter data set reprocessed over 20 years, *Ocean Sci.*, 12, 1067–1090, <https://doi.org/10.5194/os-12-1067-2016>,
917 2016.
- 918 Rentschler, J., Avner, P., Marconcini, M., Su, R., Strano, E., Vousdoukas, M., and Hallegatte, S.: Global evidence of rapid
919 urban growth in flood zones since 1985, *Nature*, 622, 87–92, <https://doi.org/10.1038/s41586-023-06468-9>, 2023.
- 920 Rojas, R., Feyen, L., and Watkiss, P.: Climate change and river floods in the European Union: Socio-economic consequences
921 and the costs and benefits of adaptation. *Glob. Environ. Change*, 23, 1737–1751.
922 <https://doi.org/10.1016/j.gloenvcha.2013.08.006>, 2013.



- 923 Sauer, I., Reese, R., Otto, C., Geiger, T., Willner, S., Guillod, B. P., Bresch, D. N., and Frieler, K.: Climate signals in river
924 flood damages emerge under sound regional disaggregation. *Nat. Commun.*, 12, 2128, [https://doi.org/10.1038/s41467-021-](https://doi.org/10.1038/s41467-021-22153-9)
925 [22153-9](https://doi.org/10.1038/s41467-021-22153-9), 2021.
- 926 Schoppa, L., Barendrecht, M. H., Paprotny, D., Sairam, D., Sieg, T., and Kreibich, H.: Projecting Flood Risk Dynamics for
927 Effective Long-term Adaptation, *Earth's Future*, accepted in print, 2024.
- 928 Scussolini, P., Luu, L. N., Philip, S. Y., Berghuijs, W. R., Eilander, D., Aerts, J. C. J. H., Kew, S. F., van Oldenborgh, G. J.,
929 Toonen, W. H. J., Volkholz, J., Coumou, D.: Challenges in the attribution of river flood events, *WIREs Climate Change*, e874.
930 <https://doi.org/10.1002/wcc.874>, 2023.
- 931 Steinhausen, M., Paprotny, D., Dottori, F., Sairam, N., Mentaschi, L., Alfieri, L., Lüdtke, S., Kreibich, H., and Schröter K.:
932 Drivers of future fluvial flood risk change for residential buildings in Europe, *Global Environ. Chang.*, 76, 102559,
933 <https://doi.org/10.1016/j.gloenvcha.2022.102559>, 2022.
- 934 Taburet, G., Sanchez-Roman, A., Ballarotta, M., Pujol, M.-I., Legeais, J.-F., Fournier, F., Faugere, Y., and Dibarboue, G.:
935 DUACS DT2018: 25 years of reprocessed sea level altimetry products, *Ocean Sci.*, 15, 1207–1224, [https://doi.org/10.5194/os-](https://doi.org/10.5194/os-15-1207-2019)
936 [15-1207-2019](https://doi.org/10.5194/os-15-1207-2019), 2019.
- 937 Tellman, B., Sullivan, J. A., Kuhn, C., Kettner, A. J., Doyle, C. S., Brakenridge, G. R., Erickson, T. A., and Slayback, D. A.:
938 Satellite imaging reveals increased proportion of population exposed to floods, *Nature*, 596, 80–86,
939 <https://doi.org/10.1038/s41586-021-03695-w>, 2021.
- 940 Thiemig, V., Gomes, G. N., Skøien, J. O., Ziese, M., Rauthe-Schöch, A., Rustemeier, E., Rehfeldt, K., Walawender, J. P.,
941 Kolbe, C., Pichon, D., Schweim, C., and Salamon, P.: EMO-5: a high-resolution multi-variable gridded meteorological dataset
942 for Europe, *Earth Syst. Sci. Data*, 14, 3249–3272, <https://doi.org/10.5194/essd-14-3249-2022>, 2022.
- 943 Tilloy, A., Paprotny, D., Grimaldi, S., Gomes, G., Bianchi, A., Lange, S., Beck, H., and Feyen, L.: HERA: a high-resolution
944 pan-European hydrological reanalysis (1950–2020), *Earth Syst. Sci. Data Discuss.* [preprint], [https://doi.org/10.5194/essd-](https://doi.org/10.5194/essd-2024-41)
945 [2024-41](https://doi.org/10.5194/essd-2024-41), in review, 2024.
- 946 Treu, S., Muis, S., Dangendorf, S., Wahl, T., Oelmann, J., Heinicke, S., Frieler, K., and Mengel, M.: Reconstruction of hourly
947 coastal water levels and counterfactuals without sea level rise for impact attribution, *Earth Syst. Sci. Data Discuss.* [preprint],
948 <https://doi.org/10.5194/essd-2023-112>, accepted in print, 2023.
- 949 U.S. Army Corps of Engineers: Coastal Engineering Manual, EM 1110-2-1100, Department of the Army, Washington D.C.,
950 2002.
- 951 van der Knijff, J.: LISVAP– Evaporation Pre-Processor for the LISFLOOD Water Balance and Flood Simulation Model, User
952 Manual, Office for Official Publications of the European Communities, Luxembourg, <https://dx.doi.org/10.2788/26160>, 2006.
- 953 Vogt, J.V., Soille, P., De Jager, A., Rimaviciute, E., Mehl, W., Foisneau, S., Bodis, K., Dusart, J., Paracchini, M., Haastруп,
954 P., and Bamps, C.: A pan-European River and Catchment Database, Publications Office of the European Union, Luxembourg,
955 <https://dx.doi.org/10.2788/35907>, 2007.



- 956 Vousdoukas, M. I., Athanasiou, P., Giardino, A., Mentaschi, L., Stocchino, A., Koop, R. E., Menéndez, P., Beck, M. W.,
957 Ranasinghe, R., and Feyen, L.: Small Island Developing States under threat by rising seas even in a 1.5 °C warming world,
958 *Nat. Sustain.*, <https://doi.org/10.1038/s41893-023-01230-5>, 2023.
- 959 Vousdoukas, M. I., Mentaschi, L., Voukouvalas, E., Bianchi, A., Dottori, F., and Feyen, L.: Climatic and socioeconomic
960 controls of future coastal flood risk in Europe, *Nat. Clim. Change*, 8, 776-780, <https://doi.org/10.1038/s41558-018-0260-4>,
961 2018.
- 962 Vousdoukas, M. I., Mentaschi, L., Voukouvalas, E., Verlaan, M., and Feyen, L.: Extreme Sea levels on the rise along Europe's
963 coasts, *Earth's Future*, 5, 304–323, <https://doi.org/10.1002/2016ef000505>, 2017.
- 964 Vousdoukas, M. I., Voukouvalas, E., Annunziato, A., Giardino, A., and Feyen, L.: Projections of extreme storm surge levels
965 along Europe. *Climate Dynamics*, 47, 3171-3190, <https://doi.org/10.1007/s00382-016-3019-5>, 2016a.
- 966 Vousdoukas, M. I., Voukouvalas, E., Mentaschi, L., Dottori, F., Giardino, A., Bouziotas, D., Bianchi, A., Salamon, P., and
967 Feyen, L.: Developments in large-scale coastal flood hazard mapping, *Nat. Hazards Earth Syst. Sci.*, 16, 1841–1853,
968 <https://doi.org/10.5194/nhess-16-1841-2016>, 2016b.
- 969 Wada, Y., Flörke, M., Hanasaki, N., Eisner, S., Fischer, G., Tramberend, S., Satoh, Y., van Vliet, M. T. H., Yillia, P., Ringler,
970 C., Burek, P., and Wiberg, D.: Modeling global water use for the 21st century: the Water Futures and Solutions (WFaS)
971 initiative and its approaches, *Geosci. Model Dev.*, 9, 175–222, <https://doi.org/10.5194/gmd-9-175-2016>, 2016.
- 972 Wing, O. E. J., Smith, A. M., Marston, M. L., Porter, J. R., Amodeo, M. F., Sampson, C. C., and Bates, P. D.: Simulating
973 historical flood events at the continental scale: observational validation of a large-scale hydrodynamic model, *Nat. Hazards*
974 *Earth Syst. Sci.*, 21, 559–575, <https://doi.org/10.5194/nhess-21-559-2021>, 2021.
- 975 Zanaga, D., Van De Kerchove, R., De Keersmaecker, W., Souverijns, N., Brockmann, C., Quast, R., Wevers, J., Grosu, A.,
976 Paccini, A., Vergnaud, S., Cartus, O., Santoro, M., Fritz, S., Georgieva, I., Lesiv, M., Carter, S., Herold, M., Li, Linlin,
977 Tsendbazar, N.E., Ramoino, F., Arino, O.: ESA WorldCover 10 m 2020 v100 [dataset],
978 <https://doi.org/10.5281/zenodo.5571936>, 2021.